Review and descriptive investigation of the connection between bipedal locomotion and non-prehensile manipulation

Yousef Farid[a], Bruno Siciliano[a], Fabio Ruggiero[a]

[a] *PRISMA Lab, Department of Electrical Engineering and Information Technology, University of Naples Federico II, Via Claudio 21, 80125, Naples, Italy*

Abstract

This paper investigates the connection between non-prehensile manipulation, specifically juggling, and legged locomotion, focusing on biped robots. In this direction, the hybrid nature of juggler robot dynamics and biped robots, the zero moment point stability, and the non-prehensile dynamic grasping conditions are provided and analysed. The similarities between juggling actions and bipedal robot locomotion are discussed. The descriptive and mathematical analysis demonstrates many similitudes between juggler systems with cubic objects and flat-feet biped robots in throwing, catching, and stabilisation phases, and between juggler actions with impact and point-feet legged robots in their switching (hybrid) dynamic behaviours. Finally, a common control framework based on the zero dynamic concept and integral sliding mode approach is proposed, and it applies to both classes of non-prehensile juggler systems and biped robots. To test the performance of the devised control system, a three-degrees-of-freedom juggler robot and a two-link walker are selected as case studies, whose simulation results demonstrate the effectiveness and feasibility of the proposed unified control framework for both systems.

Keywords: Biped robots, Non-prehensile manipulation, Juggling tasks, Hybrid dynamics, ZMP stability, Dynamic grasping conditions.

1. Introduction

Bipedal locomotion and dynamic object manipulation, including non-prehensile manipulation, are pivotal and fundamental subjects in robotics (Ryu and Lynch (2018); Khadiv et al. (2020)). Extracting the connections between these two topics may lead to directly adopting ideas and methods developed in the manipulation area to solve problems in the locomotion domain and vice versa (Akbarimajd et al. (2011)). These connections could be very beneficial in enhancing motion planning frameworks, control strategies, stability criteria, and mechanical structure in both domains.

A mobile robot is capable of autonomous locomotion around the environment, and it can be used for large workspace applications. However, the environment may be filled with obstacles or other moving robots and/or humans. Then, the robot must plan collision-free paths unless some cooperation with other robots and/or humans is desired. The use of legged robots over standard wheeled robots improves mobility over rough and uneven terrains: legs isolate the body from terrain irregularities and avoid undesirable footholds. Walking can be defined as a locomotion gait of a biped where the feet are lifted alternatively while at least one foot is always on the ground. The pioneering works in the field of legged robotics were achieved around 1970. This means that walking is younger than other robotic branches. Kajita and Espiau (2008) and Wieber et al. (2016) presented a brief history of legged robotics. Many approaches are proposed in the literature to deal with legged robotics problems (Morlando et al., 2021; Farid et al., 2021; Yeganegi et al., 2022; Farid and Ehsani-Seresht, 2021; La Hera et al., 2013). From a mechanical point of view, walking is when periodic internal shape changes of the mechanical structure, combined with reaction forces from the ground, resulting in an overall displacement. Suppose through active control of a fully actuated robot it is possible to ensure that the centre of mass (CoM) is always located above the foot area. In that case, the robot can achieve stable walking if movements are languid. This is called static walking, and the control problem is reduced to traditional joint tracking control of a rigid mechanism. The concept can be extended to the dynamic analysis of the so-called zero moment point (ZMP) in which the centre of pressure, resulting from gravitation and inertial effects, is required to remain strictly inside the support polygon (Duindam and Stramigioli, 2009; Farid et al., 2018). No matter what control technique is used, the behaviour of legged robots remains challenging to understand due to the highly nonlinear coupled, and generally unstable, dynamics together with the hybrid aspects of switching between the feet on the ground (switching between contact and no contact).

Multi-fingered object manipulation has been well formalised for many decades as evident from the works by Mason and Salisbury (1985), Murray et al. (1994), Bicchi and Kumar (2000), and Okamura et al. (2000). An object is manipulated in a non-prehensile way when it is not directly caged between the fingertips or the hands palm, and the force closure constraint does not hold (Ruggiero et al., 2018a). The grasp is then performed

Email addresses: yousef.farid@unina.it (Yousef Farid), bruno.siciliano@unina.it (Bruno Siciliano), fabio.ruggiero@unina.it (Fabio Ruggiero)

by exploiting only unilateral constraints, allowing the object to roll, slide, and break the contact with the robot manipulating it. From a robotic point of view, most non-prehensile manipulation systems are underactuated, raising controllability challenges. However, dynamic non-prehensile manipulation benefits several advantages such as the increase of available robot actions, bigger operative workspaces, and enhanced dexterity in dynamic tasks (Ruggiero et al., 2018b). Pushing objects, folding clothes, bringing a wine glass on a tray, cooking in a pan, and so on are all examples of non-prehensile manipulation actions in everyday life. Non-prehensile manipulation can also be endorsed as dynamic when the dynamics of both the object and the robot are essential to carry out the task successfully.

Johnson et al. (2012) found the duality between a multi-fingered grasp and a multi-legged stance to establish the correctness of the controller by a quasi-static analysis borrowed from the robot manipulation literature. Therefore, under certain conditions, it is possible to assume that locomotion is a kind of manipulation. Exploiting this concept, Beigzadeh et al. (2008) found out a unified approach to multi-contact planning and control at an abstract level. For static walking, it is possible to imagine that the biped robot instantaneously manipulates the planet earth, as well as a sphere (the earth) can be manipulated by two fingertips (the feet). Such an example is not, of course, what happens: to any reasonable level of precision, the robot is neither moving the world nor the world is moving the robot. Nevertheless, the problems (walking and manipulation) are similar enough that matching as closely as possible the modelling decisions (emerging from this very successful and mature body of work) facilitates the reuse of several valuable ideas and results (Johnson and Koditschek, 2013). Hence, similarities between walking and manipulation have led to several control techniques trying to optimise the contact forces between the legs and the ground as a quasi-static manipulation problem, well known in the robotics literature.

However, static walking is not well suited for fast and efficient walking. The idea is to find and establish a different connection: multi-contact dynamic and energy-efficient walking gaits must be related to non-prehensile manipulation. Indeed, agile and dexterous walking and non-prehensile manipulation share a common hybrid nature, while dynamics is crucial in both aspects. Examining this connection might bring new insights into the research community.

The following section will further expand the analysis of related work in bipedal locomotion and non-prehensile manipulation, focusing on the preliminary studies investigating the connection between the two subjects. The following section also provides the contributions of this paper. An introduction to non-prehensile manipulation, with other examples, is given in Section 3. This last also presents the dynamic equations of some robotic systems with impacts. Section 4 includes subjects related to the biped robots with both shaped and point feet. In Section 5, dynamical similarities between juggling and locomotion from different aspects are investigated. Designing a common control system framework for Lagrangian systems under sequences of impacts is presented in Section 6. Section 5 concludes this study.

2. Related work and contributions

2.1. Non-prehensile manipulation

Ruggiero et al. (2018b)) figured out that the conventional way to cope with a non-prehensile dynamic manipulation task is to split it into simpler subtasks, usually referred to as *non-prehensile manipulation primitives*. Therefore, the object is manipulated by pushing, pivoting, sliding, juggling, batting, rolling, etc. The non-prehensile manipulation approach has some advantages, such as transferring objects out of the robots workspace, eliminating the need for compliance control and finger coordination in establishing a stable grasp, reducing task execution time, and improving dexterity in dynamic tasks. Some non-prehensile manipulation tasks exhibit non-smooth dynamics (Brogliato (2016)). The robot manipulates the object through a set of contacts. When one or more of the contacts changes its mode, say from sticking contact to slipping or from slipping to no-contact, the dynamics of the system changes in a non-smooth manner. Some of these switches can be controlled, as when a finger pushing an object moves away and re-contacts it at another location or when an impact is used for control. Other switches are uncontrolled, as when the friction force between an object and a surface it is sliding on changes due to indeterminacy in the support force distribution. This kind of uncertainty is inherent in many manipulation systems. Finally, both object geometry and robot geometry are essential. Since forces are applied to the object through contact, the set of available contacts afforded by the object's geometry is critical in determining the controllability of the object and in designing a control law. Brogliato (2016) provided the entire discussion about non-smooth mechanics, including models, dynamics, and control.

Therefore, there exist three crucial control problems in non-prehensile manipulation systems.

1. Defining sensible and testable notions of controllability. The state-space of a manipulation system naturally decomposes into a robot state space and an object state space, and we are typically interested in the local and global controllability properties of the object. Some progress has been made for stratified systems by Goodwine and Burdick (2000).

2. Trajectory generation. Given the non-smooth dynamics of some manipulation systems, the problem is to find a set of controls yielding a feasible trajectory between the initial state and the goal state (Akella et al. (2000)).

3. Stabilizing a planned trajectory or equilibrium. The problem of positioning and orienting an object is to find a control law to stabilize an equilibrium.

Among the non-prehensile manipulation primitives, we focus on the batting and juggling ones. Bat-juggling is the process of manipulating an object, usually a ball, by a series of impacts with moving the object in ballistic flight between two rockets. A typical goal of a juggling system is to stabilize the desired

limit cycle. Brogliato and Rio (2000) defined the term "controllable through the impacts" to describe juggling controllability of an object. Spong (2001) considered the controllability of a batted air hockey puck instead. Control laws for juggling planar pucks and balls in space, and experimental implementations, are described by Buhler et al. (1994) and Lynch et al. (2001). Brogliato and Rio (2000)) outlined a general framework for studying juggling systems. Serra et al. (2017) proposed a nonlinear least squares approach to deal with dual-hand robotic ball juggling. Most of the juggling systems are classic examples of non-smooth dynamics. Frameworks for modeling and analysis of such systems have been proposed in the literature, including systems with unilateral constraints (Brogliato (2016); Brogliato and Rio (2000)), measure differential inclusions (Moreau (1988)), systems with perfect elastic impacts (Guckenheimer and Holmes (1983); Luck and Mehta (1983); Sanfelice et al. (2007)), and hybrid systems (van der Schaft and Schumacher (2000); Goebel et al. (2009)).

2.2. Bipedal locomotion

There has long been an interest in understanding bipedal locomotion and walking control, not only from the desire to build biped robots to perform tasks that are dangerous or degrading to humans (Johnson et al. (2017)), but also to serve as service robots (Zhu et al. (2021)), help rehabilitate people (Zhao et al. (2017)), and other aims (Chen et al. (2021)). Common approaches to locomotion control include:

- the use of passive walking as a starting point for the design of active walkers;
- the use of ZMP control;
- the use of a fixed control architecture and the application parameter search to find the parameters that yield successful walking gaits;
- the development of feedback laws based upon insights into balance and locomotion.

Walking humanoids are unstable and underactuated, and their control involves high-dimensional states and high-dimensional actions. Locomotion involves joint limit constraints, torque-limit constraints, contact constraints, and contact impacts. Also, locomotion may have several contradictory goals, including robustness and energy usage. Therefore, performing biped locomotion of humanoid robots is a challenging task. Simplified models are instrumental in producing natural motions at different walking speeds, and resembling human locomotion. Xie et al. (2021) proposed a linear inverted pendulum model (LIPM) to generate the walking reference trajectory during the single support phase. They also adopted a linear pendulum model (LPM) to describe the motion in the double support phase. Bae and Oh (2018) designed a biped robot state estimation framework based on the compliant inverted pendulum model (IPM) and a dual-loop Kalman filter estimator. Using a cart-table model, Joe and Oh (2018) proposed a balance recovery algorithm based on model predictive control. Although simpler models are more practical, most of them do not consider the nonlinear dynamics and impulsive effects in the controller design and the stabilization of periodic orbits.

Several authors adopted hybrid models to the biped robots to consider the impulsive effects. An energy shaping control method has been proposed by Arpenti et al. (2021), which guarantees that the total energy of the planar biped robots converges smoothly to the target limit cycle. Ames et al. (2014) applied an input-output feedback linearization technique, with exponentially stabilizing control Lyapunov functions, to the particular class of hybrid models with impulse effects. Designing stable walking gaits for biped robots over variable-inclined terrain using hybrid zero dynamics control framework to achieve hybrid invariant was instead presented by Horn et al. (2020).

Although many advanced results on biped walking have been reported in the literature, challenging issues, such as robust and optimal motion planning for agile locomotion, rigid movement and anti-disturbance ability, and control of the under-actuated robots represented by a class of hybrid systems when the interaction impacts affect the walking stability, are still present and need to be discussed. All these observations motivate the current study.

2.3. Connection between non-prehensile manipulation and legged locomotion

Literature review reveals that many researchers have already started investigating the notion of correspondences between non-prehensile object manipulation and legged robots but as separate topics (Kant and Mukherjee, 2022; Nguyen and Olaru, 2013; Kant and Mukherjee, 2020). Besides, Zhang et al. (2020) wrote an interesting work about the use of dynamic forces for motion generation.

Some studies focused, instead, on the analogies between non-prehensile manipulation and locomotion at the same time. Buhler et al. (1990) demonstrated that their juggler and Raiberts hopper settle down to a characteristic steady-state pattern because that pattern is an attracting periodic orbit of the closed-loop robot-environment dynamics. Klavins and Koditschek (2001) developed a coupled hybrid oscillatory method: a paddle juggling system and Raiberts hopping robot were chosen as two case studies. Beigzadeh et al. (2008) showed that simultaneous increasing the mass and dimensions of the spherical object manipulated by two arms and decreasing the earths mass and diameter leads to the unification of dynamic object manipulation and dynamic locomotion. Ramirez-Alpizar et al. (2012) proposed a dynamic non-prehensile manipulation strategy to rotate a thin deformable object on a rigid two degrees of freedom plate. They explored that the objects rotational behaviour changes with respect to the plates motion frequency, similar to a biped transitioning from sliding to walking to a running gait. Examining the connections between juggler systems and legged robots in different manipulation/locomotion phases and transition between these two tasks under other conditions needs profound research studies.

Hybrid systems with parameters or state jumps are successfully employed in representing the intricate and latent features of real mechanical systems in engineering applications where

short pulse-like signals mediate the interactions (Asano, 2015; Turki et al., 2020; Gritli, 2019; Michel et al., 2005; Michel, 1999). For a ball-playing juggling robotic system, Farid and Ruggiero (2021) showed that the juggling system could be characterised by a hybrid/switching dynamics. In such a system, ball motion is controlled by the impacts inserted by the juggler to the ball repetitively. Nguyen and Olaru (2013) investigated hybrid modelling and constrained control of another kind of juggling system. On the other hand, a nonlinear hybrid system describes the dynamic behaviour of legged robots having multi-phase properties given by the swing and stance phases of the legs (Hamed and Ames (2020); Ma et al. (2019); Martin and Gregg (2017)). The impulse effect is caused by the legs hitting the walking surface and environmental constraints.

Stability analysis and control of hybrid systems have received the attention of many researchers in the last decade (Kvlcm et al. (2021); Zeng et al. (2021); Zhang et al. (2021)). Kamidi et al. (2021) developed a distributed control algorithm based on decomposition, hybrid zero dynamics (HZD), and a scalable optimization for hybrid models of collaborative human-robot locomotion. Arcos-Legarda et al. (2019) presented a robust compound control strategy to produce a stable gait in bipedal robots with hybrid dynamics under random perturbations.

2.4. Contributions

The general discussion in our research work is that, at a mathematical level, the dynamic equations of non-prehensile juggling systems and legged robots can be represented by Lagrangian systems with hybrid dynamics. The word "hybrid" is here employed as by (Di Bernardo et al., 2008), where a set of ordinary differential equations plus a set of reset maps is referred to as a piecewise-smooth hybrid system, here shortened for the rest of the paper as hybrid system. We can push the control technologies from the non-prehensile manipulation domain to the locomotion field and vice versa, where well-known controllers can be reused to solve the task and see the performance of the designed solution. Consequently, locomotion and non-prehensile juggling manipulation will be tackled as a unified problem, allowing simultaneous and coordinated execution of both tasks.

The contribution points of this research study are given in the following.

i) Identify a set of common characteristics between different phases of flat-feet biped robots and non-prehensile juggling systems such as throwing, free-flight-catching, and balancing are investigated.

ii) It is proven that the stability conditions in the support phase of a flat-feet biped robot have a similar structure of dynamic grasp conditions in the carrying phase of a juggling system.

iii) A unified optimisation problem is formulated for the throwing phase of the biped robot locomotion and dynamic object manipulation, where the output of the algorithm is the optimal trajectory of biped robot's CoM and the manipulated object's CoM.

iv) The connections between point-foot biped robots and juggling with impacts are verified.

v) A control system using zero dynamic-based integral sliding mode controller is designed for the general class of juggler/biped robots with hybrid Lagrangian dynamics.

vi) Stability analysis based on Lyapunov theory ensures that the controlled nonlinear hybrid robotic system is finite-time stable under the sequences of impacts.

3. Non-prehensile manipulation

In daily human routine, some activities require strength, skill, thinking, assessment, and dexterity to be done correctly. In some tasks, people manipulate objects in interesting ways that do not involve grasping. Pushing a car to start it is a tangible and understandable example of moving objects without grasping. To move the vehicle, a resultant force with an appropriate amplitude that causes the car to move must be applied in the direction of the surface on which the vehicle is located (Fig. 1(a)). In the pizza-making process, for instance, dynamic non-prehensile manipulation consists of rotating/translating a rigid body (plate) and a deformable body (pizza dough with other ingredients) and also sliding manipulation, in which dynamic effects generate the objects deformation (Fig. 1(b)). In a basketball game, the ball is thrown by the attacking player towards the goal, which the target is the basket of the opposing team. The vision, centralisation, angle of throwing, and the power of arms of the attacking player play essential roles in reaching the ball to the basket (Fig. 1(c)). Continuous manipulation of a ball rolling around a butterfly device needs concentration, visual feedback, and high-speed action. Although its mechanism may look likes simple, in practice doing so is challenging for humans (Fig. 1(d)). Another non-prehensile action in which the object moves a long distance without grasping is batting, like in the baseball game. Good pre-pitch rhythms of the body, arms, and legs of the player ensure success in the game (Fig. 1(e)). Juggling is a physical skill performed by a juggler involving manipulating objects for recreation, entertainment, art, or sport. The most recognizable form of juggling is toss juggling (Fig. 1(f)). Juggling can be the manipulation of one or many objects simultaneously, most often using one or two hands but also possible with feet. Jugglers often refer to the objects they juggle as props. The most common props are balls, clubs, or rings. Some jugglers use more dramatic objects such as knives, fire torches, or chainsaws. The term juggling can also commonly refer to other prop-based manipulation skills, such as diabolo, plate spinning, devil sticks, poi, cigar boxes, contact juggling, hooping, yo-yo, and hat manipulation. All of the introduced actions are examples of non-prehensile manipulation, which means manipulation without grasping.

So far, many robotic systems have been built and trained to perform tasks that require high skill and power (such as non-prehensile tasks). As shown in Fig. 2(a), TORO humanoid

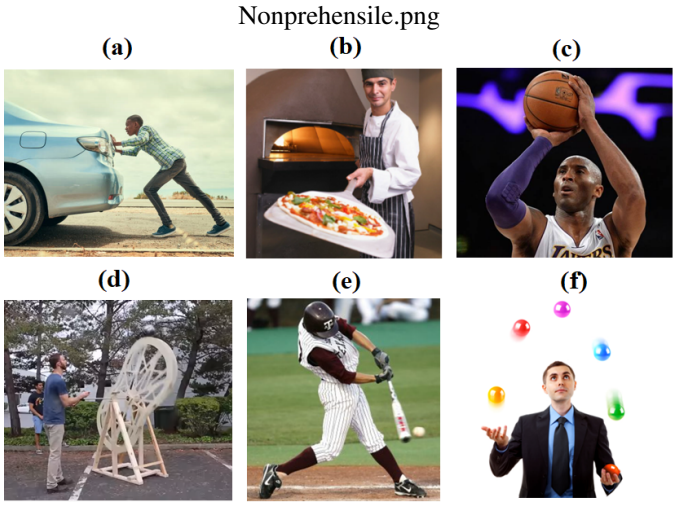

Figure 1: Non-prehensile actions by humans: (a) pushing a car (courtesy of IMG-1), (b) rotational/translation/sliding (courtesy of IMG-2), (c) throwing a ball (courtesy of IMG-3), (d) ball rolling around a butterfly device (courtesy of IMG-4), (e) batting (courtesy of IMG-5), and (f) juggling (courtesy of IMG-6).

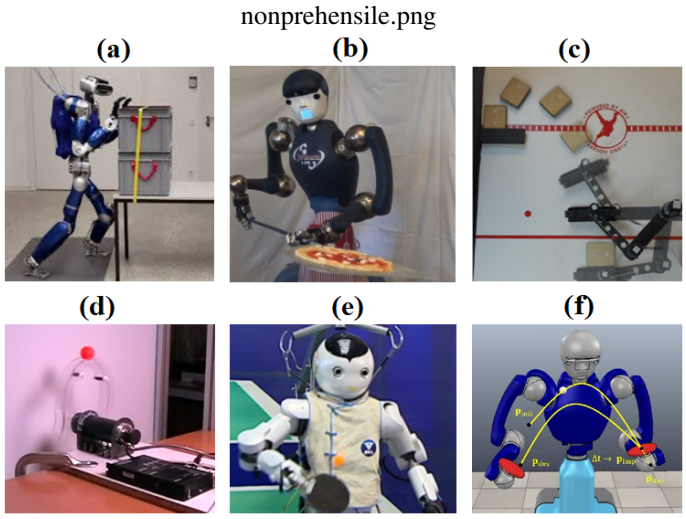

Figure 2: Non-prehensile actions by robotic systems: (a) pushing two boxes by TORO humanoid robot (courtesy of Abi-Farraj et al. (2019)), (b) RoDyMan humanoid robot (courtesy of Ruggiero et al. (2018b)), (c) throwing an object by a robotic manipulator (courtesy of Woodruff and Lynch (2017)), (d) butterfly robot (courtesy of Surov et al. (2015)), (e) ping-pong playing robot (courtesy of Su et al. (2013)), and (f) ball-juggling robotic system (courtesy of Serra et al. (2017)).

robot is pushing two boxes to the forward position on the table in a non-prehensile way. Balancing is a critical feature for a robot interacting with an unstructured environment. There, the balancing control should account for unknown perturbation forces that might destabilise the robot when performing the intended tasks (Abi-Farraj et al. (2019)). The RoDyMan project was successfully developed to mimic human behaviour for non-prehensile dynamic manipulation of rigid and deformable objects (Ruggiero et al. (2018b)) (Fig. 2(b)). Similar to the throwing actions of humans, Woodruff and Lynch (2017) developed a robotic system performing the non-prehensile throwing task (see Fig. 2(c)). A type of butterfly robot was implemented by Surov et al. (2015) for developing systematic techniques for non-prehensile rolling manipulation. Motion planning and stabilization of the robotic platform are considered as a challenging benchmark (Fig. 2(d)). Playing pingpong is one of the most challenging non-prehensile tasks (Fig. 2(e)). To perform this task, several capabilities are required for a robot system, such as smart sensing, object tracking, trajectory prediction, and motion planning (Su et al. (2013)). A dual-hand robotic system that can perform a repetitive batting of a ball between two paddles/hands in a non-prehensile way was implemented by Serra et al. (2017) (Fig. 2(f)). This robotic platform also requires the same capabilities mentioned for ping-pong player robots.

In this research, we pay attention to the juggling/batting tasks. Our primary focus will be analysing the dynamic behaviour of robotic systems subjected to the impacts. At first, two famous percussion systems under impacts, normal and inverse pendulum systems, are introduced, despite they can not be classified as non-prehensile manipulation primitives. Then, in the following section, the dynamic behaviour of a juggler system is analysed.

3.1. Dynamic equations of inverse/normal pendulums under impacts

The equations of motion for the impacting pendulums which are shown in Fig. 3(a)-(b) are as follows (Moore and Shaw (1990))

$$\begin{cases} ml^2\ddot{\theta} + b\dot{\theta} \pm mgl\sin(\theta) = lAm\omega_{d\tau}^2\cos(\theta)\cos(\omega_{d\tau}\tau), & |\theta| < \theta_{max} \\ \dot{\theta}^+ = -r\dot{\theta}^-, & |\theta| = \theta_{max} \end{cases} \tag{1}$$

where $m > 0$ and $l > 0$ are the mass and the length of the pendulum, respectively. The + (or -) sign is used for the normal (or inverted) pendulum. The parameter $A \in \mathbb{R}$ represents the amplitude of the support displacement, $b > 0$ is the effective angular viscous damping constant, $g > 0$ is gravitational acceleration, $\omega_{d\tau} > 0$ is the frequency of the input motion, $r > 0$ is the coefficient of restitution at impact, and $\tau > 0$ representing the time variable. The constraints are placed symmetrically at $\theta = \pm\theta_{max}$.

The inverted case is considered first. Defining $t = \sqrt{(J/l)}\tau$ and $\phi = \theta/\theta_{max}$, the non-dimensional equations of motion for the system are

$$\begin{cases} \ddot{\phi} + 2\alpha\dot{\phi} - \phi = \beta\cos(\omega t), & |\phi| < 1, \\ \dot{\phi}^+ = -r\dot{\phi}^-, & |\phi| = 1, \end{cases} \tag{2}$$

where $2\alpha = b/\sqrt{ml^3g}$, $\omega = \omega_{d\tau}\sqrt{l/g}$, and $\beta = A\omega_{d\tau}^2/g\theta_{max}$. The parameter α represents the non-dimensional damping ratio, β the non-dimensional driving acceleration, ω is the dimensionless driving frequency, and r is the coefficient of restitution. The non-dimensional equations of motion for the normal pendulum are

$$\begin{cases} \ddot{\phi} + 2\alpha\dot{\phi} + \phi = \beta\cos(\omega t), & |\phi| < 1, \\ \dot{\phi}^+ = -r\dot{\phi}^-, & |\phi| = 1, \end{cases} \tag{3}$$

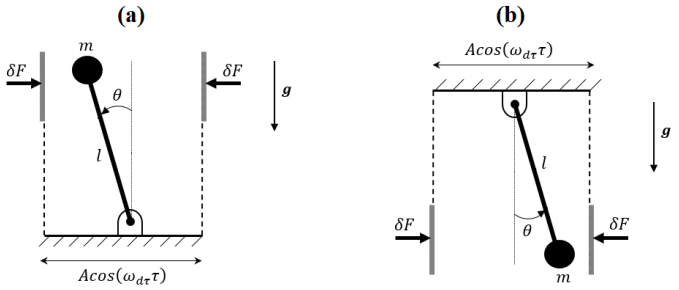

Figure 3: Impacting pendulums: (a) inverse pendulum, and (b) normal pendulum.

where the dimensionless parameters for this case are the same as for the inverted pendulum, with θ defined as in Fig. 3(b). The dynamic behaviour of the normal and inverted pendulums, equations (2) and (3), have been simulated. The parameters have been chosen as $\alpha = 0.075$, $\beta = 1.5$, $\omega = 4$, $r = 0.99$, $\phi(0) = -0.4$, and $\dot{\phi}(0) = -0.99$. The state trajectories are plotted in Fig. 4(a) and (b). The phase spaces are depicted in Fig. 5(a) and (b), respectively. Notice how ϕ and $\dot{\phi}$ have stable and periodic behaviours.

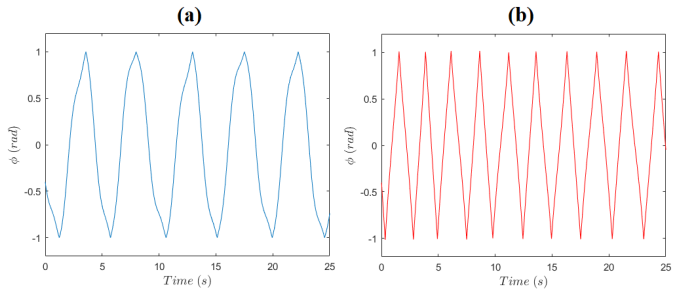

Figure 4: State response of inverse (a) and normal (b) pendulums.

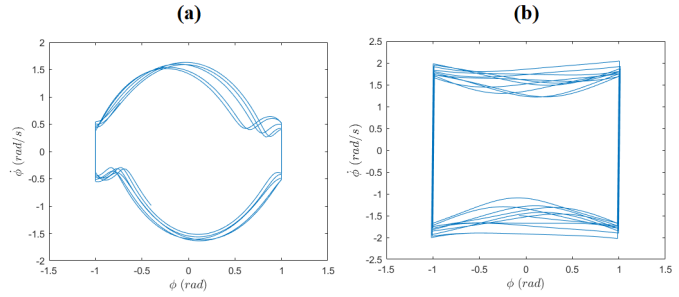

Figure 5: Phase space of inverse (a) and normal (b) pendulums.

3.2. *Dynamic equations of a three-degree-of-freedom juggling system*

Consider the case that two juggler robots with three degrees of freedom that are playing a ball (see Fig. 6). The first juggler's end-effector position can be retrieved through the following geometric relationships

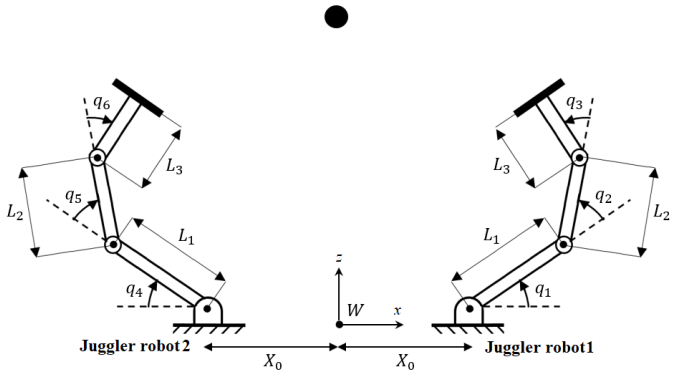

Figure 6: Geometrical structure of two juggler robots with three degrees of freedom each.

$$\begin{cases} x_e = L_1\cos(q_1) + L_2\cos(q_1+q_2) + L_3\cos(q_1+q_2+q_3) + X_0, \\ z_e = L_1\sin(q_1) + L_2\sin(q_1+q_2) + L_3\sin(q_1+q_2+q_3), \end{cases} \tag{4}$$

where $q_1, q_2, q_3 \in \mathbb{R}$ are the joint angles of the juggler robot 1, $L_1, L_2, L_3 > 0$ are the length of the links, and $X_0 \in \mathbb{R}$ is a displacement along the horizontal axis of the world frame W. Similar expressions can be obtained for the second juggler robot with the related joint angles $q_4, q_5, q_6 \in \mathbb{R}$. The dynamic equation of each juggler robot has the following form

$$M_{Ji}(q_{Ji})\ddot{q}_{Ji} + C_{Ji}(q_{Ji}, \dot{q}_{Ji})\dot{q}_{Ji} + g_{Ji}(q_{Ji}) = B_{Ji}\tau_{Ji}, \quad i = 1, 2 \tag{5}$$

where $q_{J1} = [q_1, q_2, q_3]^T$ and $q_{J2} = [q_4, q_5, q_6]^T$ are the stacking vector of each manipulator joinnts, $\dot{q}_{Ji} \in \mathbb{R}^3$ the related time derivative vector, $M_{Ji} \in \mathbb{R}^{3\times3}$, $C_{Ji} \in \mathbb{R}^{3\times3}$, and $g_{Ji} \in \mathbb{R}^3$ are called the inertia matrix, the Coriolis matrix, and the vector of gravitational terms, respectively. Also, $B_{Ji} \in \mathbb{R}^{3\times m}$ is the allocation matrix for the actuation $\tau_{Ji} \in \mathbb{R}^m$, with $0 < m \leq 3$.

For the first ball-juggler robot, the impact condition is defined with respect to the state vector q_{J1} as

$$\begin{cases} x_b - \Big[L_1\cos(q_1) + L_2\cos(q_1+q_2) + L_3\cos(q_1+q_2+q_3) \\ \qquad +X_0\Big] = 0, \\ z_b - \Big[L_1\sin(q_1) + L_2\sin(q_1+q_2) + L_3\sin(q_1+q_2+q_3)\Big] = 0, \end{cases} \tag{6}$$

where $x_b \in \mathbb{R}$ and $z_b \in \mathbb{R}$ are the position of the ball in W. Note that the similar expressions can be obtained for the second juggler robot.

Three forces affect the dynamic behaviour of the ball, with mass $m_o > 0$, during the free-flight motion, namely: the air resistance force, $f_a \in \mathbb{R}^3$, the Magnus force, $f_m \in \mathbb{R}^3$, and the gravitational force $f_g \in \mathbb{R}^3$. Following Zhang et al. (2018), we have

$$m_o\dot{v}_b = f_a + f_m + f_g, \tag{7}$$

where

$$f_a = -\frac{1}{2}\rho s_a c_a \|v_b\| v_b, \tag{8}$$

$$f_m = \rho\omega_b r_b s_a c_l v_b, \tag{9}$$

$$f_g = [0, 0, -m_o g]^T, \tag{10}$$

where $\rho > 0$ is the air density, $c_a > 0$ is the drag coefficient, $v_b = \begin{bmatrix} v_{b_x} & v_{b_y} & v_{b_z} \end{bmatrix}^T \in \mathbb{R}^3$ is the translational velocity of the ball, $\|\cdot\| > 0$ is the Eucledian norm operator, $\omega_b \in \mathbb{R}^3$ is the rotational velocity of the ball, and $c_l > 0$ is the lift coefficient. Finally, $s_a > 0$ and $r_b > 0$ are the effective contact area and radius, respectively. Therefore, again following Zhang et al. (2018), the motion of the ball can be represented by the following equations

$$\begin{bmatrix} \dot{x}_b \\ \dot{y}_b \\ \dot{z}_b \\ \dot{v}_{b_x} \\ \dot{v}_{b_y} \\ \dot{v}_{b_z} \end{bmatrix} = \begin{bmatrix} v_{b_x} \\ v_{b_y} \\ v_{b_z} \\ -\frac{1}{2m}\rho s_a (c_a \|v_b\| - 2\omega_b r_b c_l) v_{b_x} \\ -\frac{1}{2m}\rho s_a (c_a \|v_b\| - 2\omega_b r_b c_l) v_{b_y} \\ -\frac{1}{2m}\rho s_a (c_a \|v_b\| - 2\omega_b r_b c_l) v_{b_z} - g \end{bmatrix}, \tag{11}$$

where y_b is the position of the ball y direction of W.

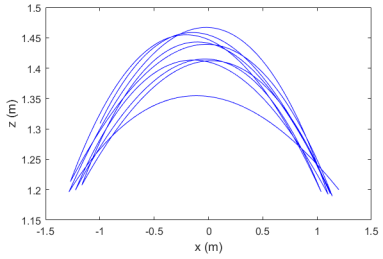

Figure 7: Measured ball motion trajectory during ball-playing game by two juggler robots. Red marker O indicates the initial position of the ball.

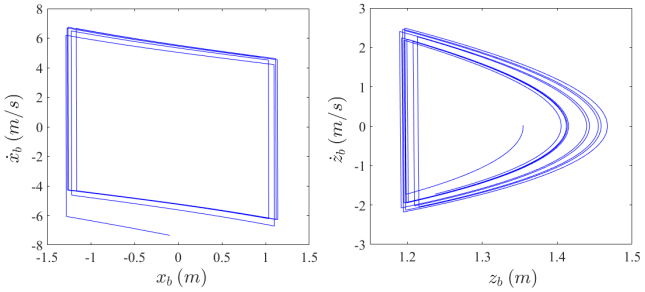

Figure 8: Phase portraits of the ball states.

After an impact, the translational and rotational velocities of the ball are updated according to the following equation (see (Serra et al., 2017))

$$v_b^+ = v_r + R_{rot} A_{vv} R_{rot}^T (v_b^- - v_r) + R_{rot} A_{vw} R_{rot}^T \omega_b^-, \tag{12}$$

$$\omega_b^+ = R_{rot} A_{wv} R_{rot}^T (v_b^- - v_r) + R_{rot} A_{ww} R_{rot}^T \omega_b^-, \tag{13}$$

where $v_r \in \mathbb{R}^3$ is the velocity of the racket attached to the juggler robot's end-effector at the hitting time, $R_{rot} \in SO(3)$ is the rotation matrix of the racket frame with respected to the world frame, $A_{vv} = \text{diag}(1 - k_v, 1 - k_v, -e_r)$, $A_{vw} = k_v r S_{rb}$, $A_{wv} = -k_w r S_{rb}$, $A_{ww} = \text{diag}(1 - k_w r^2, 1 - k_w r^2, 1)$, and

$$S_{rb} = \begin{bmatrix} 0 & 1 & 0 \\ -1 & 0 & 0 \\ 0 & 0 & 0 \end{bmatrix}.$$

The values of the parameters were chosen as $m_b = 2.7 \cdot 10^{-3}$, $e_r = 7.3 \cdot^{-1}$, $k_v = 6.15 \cdot 10^{-1}$, $k_w = 2.57 \cdot 10^3$, and $r = 2 \cdot 10^{-2} m$ in the carried out simulations (Zhang et al. (2018)). The measured ball motion trajectory (the so-called juggling pattern) is plotted in Fig. 7 in the $x - z$ plane of W. It is observed that the juggling pattern results in the desired repetitive action for the whole playing time. The phase portraits of the ball states are plotted in Fig. 8. These figures confirm the hybrid nature of ball motion and periodic behaviour in the steady-state.

3.3. Juggling motions with shaped end-effector and shaped objects

Non-prehensile dynamic manipulation of polygonal or shaped objects by robotic arms is studied from kinematics and planning viewpoints. In the studied manipulation methods, given a goal position, an object's required release position and velocity are determined for throwing. Then, the object is manipulated to its goal configuration. Dynamic actions are throwing, hitting, catching, and grasping. A robot system needs to perform such activities to realize dexterous and flexible manipulation. One of the characteristics of such movement is that the robot can manipulate an object quickly. The important thing is for the robot to know that higher speed is required.

A structure of a humanoid robot that performs juggling manipulation is shown in Fig. 9(a). The car juggler humanoid robot is equipped with a high-resolution camera, multi-finger hands, a strong data/signal processing processor, good mechanical structure, and high-speed servo valves. A diesel engine will generate hydraulic pressure, and the mobility required for juggling the cars will come from hydraulic accumulators. Four mentioned dynamic actions are realized in this test-bed. Some interesting robotic platforms have been implemented to perform juggling actions with shaped objects and different shape end-effectors. Erumalla (2018) implemented the contact juggling manipulation of a disk with a disk-shaped manipulator, called the mobile disk-on-disk. The system consists of two disks in which the upper disk (object) is free to roll on the lower disk (hand) under the influence of gravity (Fig. 9(b)). The throwing, catching, and balancing of an object has been studied in this experiment. As shown in Fig. 9(c), 1-DOF juggling prismatic robotic system simulated in ADAMS. The shape of the object is cubic, and Akbarimajd (2009) proposed an optimization algorithm for finding optimal flight height. For solving dynamic catching, a new box-like end-effector for juggler robotic systems (Fig. 9(d)) was proposed by (Schill and Buss (2018)), showing that the end-effector shape reduces contact surface with the ball and thus avoids jamming. Spherical objects are automatically driven to the throwing position, while cuboids must be placed manually.

juggler.png

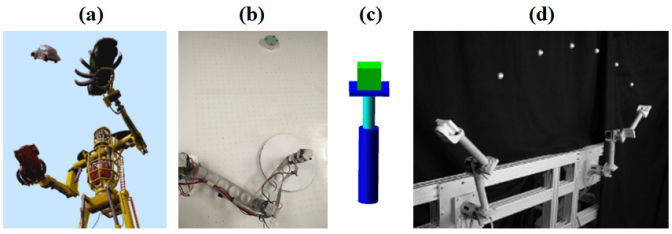

Figure 9: Different types of juggler robotic systems with shaped end-effector and shaped objects: (a) a car-juggling humanoid robot (courtesy of IMG-7), (b) juggling a disk with a disk-shaped end-effector by using a two-link manipulator (courtesy of Erumalla (2018)), (c) a one-degree-of-freedom prismatic joint arm manipulating a cubic object (courtesy of Akbarimajd (2009)), (d) two symmetric robots perform juggling action (courtesy of Schill and Buss (2018)).

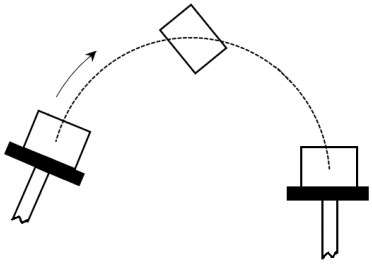

and catching.png

Figure 10: Throwing and catching of an object.

We consider a two-juggler robotic manipulator that repeatedly throws and catches an object in a gravity field (Fig. 10). A "catch" consists of letting the object impact the palm mounted in the end-effector of the juggler and come to rest. By proper choice of the thrown velocity and the geometry of the arm, a unique recurrent motion pattern of the object emerges. This behavior appears without sensing a large set of initial configurations of the part. Instead of collapsing the possible part configurations to a single point, the device collapses the initial configurations into a cycle similar to a stable limit cycle.

4. Dynamic behaviors of bipedal robots

A biped robot is an open kinematic chain consisting of two sub-chains called legs and the torso, all connected at a common point called the hip. One or both legs may be in contact with the ground. When only one leg touches the ground, the contacting leg is called the "stance" or "support" leg, while the other is referred to as the "swing" leg. The end of a leg will sometimes be referred to as the foot. The single support or swing phase is defined as the locomotion where only one foot is on the ground. Conversely, the double support is the case in which both feet are on the ground. Walking is then defined as alternating phases of single and double support. The requirement is that the displacement of the horizontal component of the robots center of mass (COM) is strictly monotonic. Running is defined as sequential phases of single support, flight, and (single-legged) impact, with the additional provision that impacts occur on alternating legs.

foot biped.png

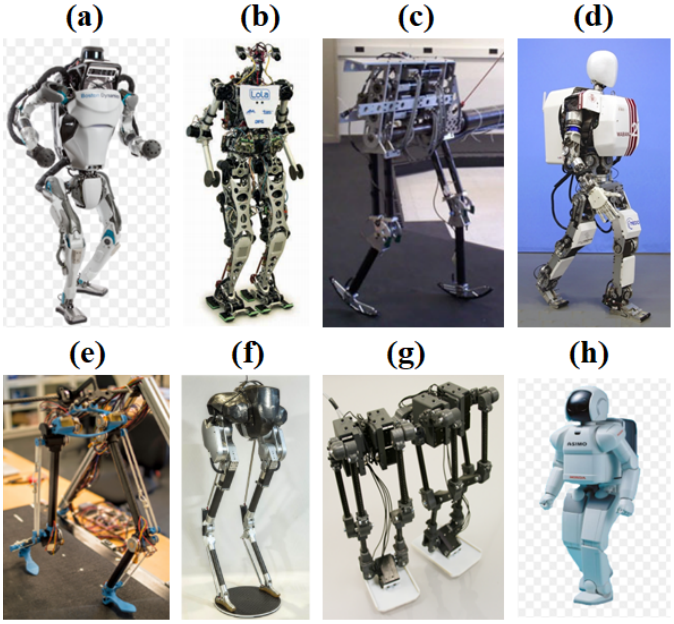

Figure 11: Different types of shaped foot bipedal/humanoid robots: (a) ATLAS (courtesy of IMG-ATLAS), (b) LOLA (courtesy of IMG-LOLA), (c) ERNIE (courtesy of Fevre et al. (2018)), (d) WABIAN-2R (courtesy of IMG-WABIAN), (e) RuBi (courtesy of IMG-RuBi), (f) Cassie (courtesy of Duan et al. (2021)), (g) a typical biped robot with hybrid leg mechanism (courtesy of Gim et al. (2018)), and (h) ASIMO (courtesy of IMG-ASIMO).

Foot and ankle are critical structural components of a biped robot. Their proper design is a decisive factor in creating the correct gait and ensuring these robots' walking/running stability. Looking at the legged robots literature, bipeds have been studied in two separate categories: bipedal robots with shaped feet and point-foot bipedal robots. We pay attention to these two types of biped robots and their related issues in the following.

4.1. Shaped-foot bipedal robots

Laboratories around the world have produced many different types of bipedal/humanoid robots with shaped feet, such as ATLAS, LOLA, ERNIE, WABIAN-2R, RuBi, Cassie (Duan et al. (2021)), a typical biped robot with a hybrid leg mechanism, and ASIMO (Fevre et al. (2018); Gim et al. (2018)). These biped robots are shown in Fig. 11(a)-(h).

A mechanical model is "fully actuated" when the number of independent actuators equals the number of degrees of freedom (Westervelt et al. (2007)). If there are fewer actuators than degrees of freedom, it is "underactuated". If there are more actuators than degrees of freedom, it is "overactuated" or "redundant". A biped robot in single support is fully actuated if it has a stationary stance foot (i.e., flat on the ground and neither rotating nor slipping (Fig. 12(a)), and all of the joints of the robot are actuated; otherwise, the robot is underactuated. In particular, notice that a fully actuated robot (i.e., a robot with feet and all joints actuated) is underactuated in the case the heel rises and the foot rotates about the toe (Fig. 12(b)). Whenever non-flat-footed walking takes place, underactuation is present.

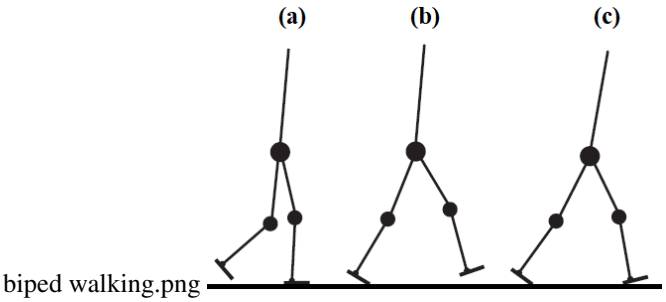

Figure 12: Various phases of bipedal walking with non-point feet. The single support phase (also called the swing phase) is shown in (a) and (b), while a double support phase is depicted in (c). If all of the joints of the robot are actuated and the feet are not slipping, then comparing the number of degrees of freedom to the number of independent actuators reveals that the robot is fully actuated in (a), under-actuated in (b), and over-actuated in (c) (courtesy of Westervelt et al. (2007)).

The most critical and primary topic for a humanoid biped robot is its walking ability. Many factors influence the stability of walking, such as center-of-gravity (CoG) trajectory, torso posture, and the ZMP trajectory. For now, the concept of ZMP is the most popular theorem to use in achieving the criterion of stable walking. The ZMP is defined as the point on the ground at which the net moment of the inertial forces and the gravity forces has no component along the horizontal axes (Vukobratovic et al.). For kinematic chain structure, the ZMP coordinates in x- and y-direction are calculated from

$$x_{zmp} = \frac{\sum_{n=1}^{N_l} (m_i(\ddot{z}_i + g)x_i - m_i\ddot{x}_i z_i - (I_i\ddot{\theta}_i)_y)}{\sum_{n=1}^{N_l} m_i(\ddot{z}_i + g)}, \tag{14}$$

$$y_{zmp} = \frac{\sum_{n=1}^{N_l} (m_i(\ddot{z}_i + g)y_i - m_i\ddot{y}_i z_i - (I_i\ddot{\theta}_i)_x)}{\sum_{n=1}^{N_l} m_i(\ddot{z}_i + g)}, \tag{15}$$

where $m_i > 0$ is the mass of link i. The coordinates of the i-th link are described by (x_i, y_i, z_i). Correspondingly, accelerations of link i in $x-$, $y-$, and $z-$direction are represented by $\ddot{x}_i$, $\ddot{y}_i$, and $\ddot{z}_i$, respectively. $(I_i)_x > 0$ and $(I_i)_y > 0$ are the inertial components. $(\ddot{\theta}_i)_x \in \mathbb{R}$ and $(\ddot{\theta}_i)_y \in \mathbb{R}$ are the absolute angular acceleration component around $x-$ and $y-$ axes at the CoG of the i-th link. $N_l > 0$ is the number of links. According to the dynamic stability criterion defined by the ZMP (see Vukobratovic et al.), the position of ZMP should be within the stable region, which changes from the area of the standing feet to the convex polygon formulated by the two feet when gaits change from the single support to the double support phase. The ZMP trajectory and ZMP regions of biped robots with flat feet during locomotion and in single support phase and double support phase are given in Fig. 13.

Considering that the CoG has the following expressions

$$x_{cog} = \frac{\sum_{n=1}^{N_l} m_i x_i}{m}, \tag{16}$$

$$y_{cog} = \frac{\sum_{n=1}^{N_l} y_i x_i}{m}, \tag{17}$$

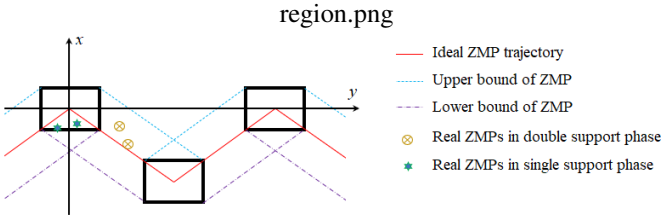

Figure 13: ZMP trajectory and ZMP regions of biped robots with flat feet.

where $m = \sum_{n=1}^{N_l} m_i$. One can rewrite equations (14) and (15) in terms of the COG equations (16) and (17) as follows

$$x_{zmp} = x_{cog} - \frac{m\ddot{x}_{cog}z_{cog} - \dot{h}_y}{m(g + \ddot{z}_{cog})}, \tag{18}$$

$$y_{zmp} = y_{cog} - \frac{m\ddot{y}_{cog}z_{cog} - \dot{h}_x}{m(g + \ddot{z}_{cog})}, \tag{19}$$

where $\dot{h}_x \in \mathbb{R}$ and $\dot{h}_y \in \mathbb{R}$ are the time derivatives of the angular momentum in x and y directions, respectively. As shown in Fig. 13, the ZMP position should by confined between upper and lower bounds. Assume that the ZMP's upper and lower bounds are specified by $(x_{zmp,u}, x_{zmp,u})$ and $(x_{zmp,l}, y_{zmp,l})$, respectively. Therefore, the stability conditions can be written as

$$x_{zmp,l} \leq x_{cog} - \frac{m\ddot{x}_{cog}z_{cog} - \dot{h}_y}{m(g + \ddot{z}_{cog})} \leq x_{zmp,u}, \tag{20}$$

$$y_{zmp,l} \leq y_{cog} - \frac{m\ddot{y}_{cog}z_{cog} - \dot{h}_x}{m(g + \ddot{z}_{cog})} \leq y_{zmp,u}. \tag{21}$$

Now, we pay attention to the issue of the friction constraint. Let $f_f = [f_{f_x}, f_{f_y}, f_{f_z}]^T \in \mathbb{R}^3$ be the contact force vector, where F_{f_x}, F_{f_y}, and F_{f_z} are the components of f_f along x, y, and z directions at the contact point, respectively. To ensure a no-slipping condition, the contact force f_{f_z} must satisfy the following contact constraint

$$\sqrt{f_{f_x}^2 + f_{f_y}^2} \leq \mu f_{f_z}, \tag{22}$$

where $\mu > 0$ is the static friction coefficient of the substrate. The friction constraint can be geometrically represented as a cone whose axis is orthogonal with respect to the support surface and with an opening angle equals to $\alpha = \arctan(\mu)$. Nonlinear constraint (22) can by approximated through

$$|f_{f_x}| \leq \mu_p f_{f_z}, \qquad |f_{f_y}| \leq \mu_p f_{f_z}, \tag{23}$$

where $\mu_p = \mu/\sqrt{(2)}$. The previous friction force constraints can be rewritten in a matrix form as follows

$$\begin{bmatrix} 1 & 0 & -\mu_p \\ -1 & 0 & -\mu_p \\ 0 & 1 & -\mu_p \\ 0 & -1 & -\mu_p \end{bmatrix} f_f \leq 0_4, \tag{24}$$

with $0_\times$ the zero vector of proper dimensions.

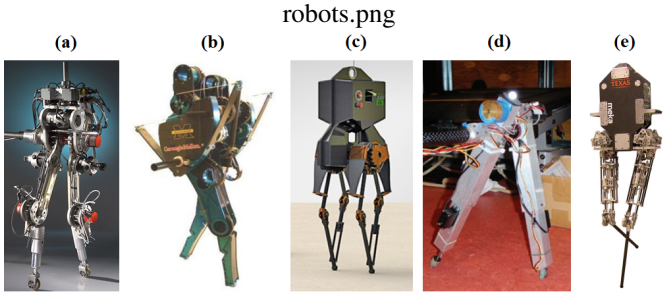

Figure 14: Different types of point foot biped robots: (a) RABBIT (courtesy of Chevallereau et al. (2003)), (b) MABEL (courtesy of Grizzle (2009)), (c) ATRIAS (courtesy of Ramezani et al. (2014)), (d) Two-link walker (courtesy of Manchester et al. (2011)), and (e) HUME (courtesy of Kim et al. (2014)).

4.2. Point-foot bipedal robots

Five well-known biped robots with point feet that attracted the focus of scholars for studying their hybrid dynamic behaviors are RABBIT, MABEL, ATRIAS, two-link walker, and HUME. They are all displayed in Fig. 14(a)-(e). RABBIT is the output of the cooperative research works of automation and robotic laboratories in France (Chevallereau et al. (2003)). MABEL is a robot engineered in 2009 by researchers at the University of Michigan, well known for being the world's fastest bipedal robot with knees. MABEL can reach speeds of up to 3.6 m/s (6.8 mph). The name MABEL is an acronym for Michigan Anthropomorphic Biped With Electronic Legs. MABEL weighs 143 lb (about 65 kg), with most of its weight being in the top torso area (Grizzle (2009)). ATRIAS represents a collaborative effort of Oregon State University, Carnegie Mellon University, and the University of Michigan. The robot has been conceived for energy efficiency, speed, and robustness with respect to natural terrain variations, without over-reliance on external sensings, such as vision (Ramezani et al. (2014)). The two-link walker was built by the Massachusetts Institute of Technology (MIT), USA (Manchester et al. (2011)). HUME is a hyper agile bipedal robot developed by Sentis's team at the University of Texas at Austin, USA (Kim et al. (2014)). This robot was designed to quickly traverse rough terrains that are at the extreme of what humans can overcome on two feet.

Hybrid systems exhibit characteristics of both continuous- and discrete-time dynamical systems and have become a compelling approach to study legged locomotion and mechanical systems subject to impacts (Grizzle et al. (2014)). Models of legged robots are hybrid with continuous-time domains representing the Lagrangian dynamics and discrete-time transitions representing the changes in physical constraints (i.e., a non-stance leg contacting the walking surface). A walking motion is a periodic orbit in a hybrid model, as evident in Fig. 15. Key elements are the continuous dynamics of the single support phase, written in state-space form as $\dot{x} = f(x) + g(x)u$, the switching or impact condition, $\vartheta(x) = 0$, which detects when the height of the swing leg above the walking surface is zero, and the reinitialization rule coming from the impact map, $x^+ = \Delta(x^-)$. In the running motion of the biped robots, switching occurs between the standing phase and free-flight phase as shown in Fig. 16, in which x_f is the state of the biped robot during free-flight, x_s is

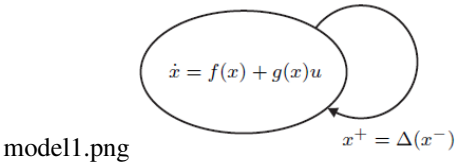

Figure 15: Single-mode hybrid model of walking that corresponds either to walking with point feet.

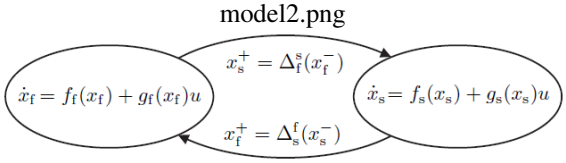

Figure 16: Double-mode hybrid model of runner point-foot biped robots.

the state of biped robot in support phase, and x_f^+ and x_s^+ are the reinitializations of the robot states.

5. Connection between non-prehensile juggling manipulation and locomotion of biped robots

We are interested in finding a dual interpretation (or a mathematical map) between bipedal locomotion and non-prehensile manipulation (particularly the batting/juggling primitive) systems. The possibility of improving the robustness of bipedal robotic systems will be thus obtained. To this end, we investigate the similarity between juggling tasks with impacts and both flat-feet and point-feet biped robot locomotion.

5.1. Connection between flat-foot bipedal robot locomotion and juggling manipulation with a flat-shaped object

The system presented in Fig. 17(a) shows a manipulation system. In this figure, the radius and the mass of the manipulated sphere are $r_0 > 0$ and $m_0 > 0$, respectively, while the planet earths radius and mass are $R_0 > 0$ and $M_0 > 0$, respectively. We can solve the manipulation problem with these parameters. Now, we are going to exchange the parameters. In other words, we gradually enlarge the radius and the mass of the sphere to R_0 and M_0 and, at the same time, we shrink the radius and the mass of the planet earth to r_0 and m_0, respectively. Consequently, the direction of the gravity vector, $g \in \mathbb{R}^3$ will be reversed. These changes eventually result in the system depicted in Fig. 17(b). Looking upside-down at Fig. 17(b), we see the system shown in Fig. 17(c), that t is a bipedal robot walking on the earth.

After sketching out this rough similarity, we go through many aspects connecting the two fields, from the path planning, the different phases of the task, to the stability criteria, etc.

5.1.1. Connection between the manipulated and locomotion path

We explain the path planning strategy for non-prehensile manipulation and locomotion through Fig. 18(a) and (b). At the beginning of each cycle, the first manipulator is ready to catch

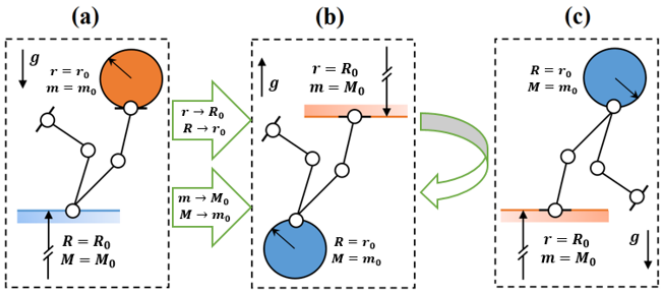

Figure 17: Duality of locomotion and non-prehensile manipulation (courtesy of Beigzadeh et al. (2008)).

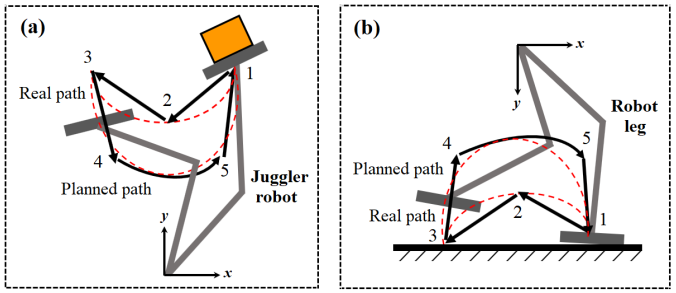

Figure 18: (a) Dynamic manipulation of a cubic flat-shaped object by a juggler robot, (b) gait pattern during the locomotion of a flat-foot biped robot with. The planned and real paths are shown by solid black and dashed red lines, respectively.

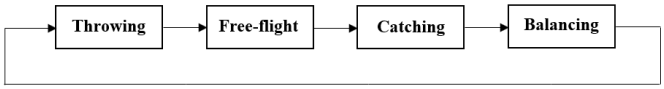

Figure 19: Object juggling and biped robot running sequences.

the object in point 1. Sensing the first impact signal, the controller switches to smaller gains. Hence, the whole manipulator accommodates the object's motion (apparent low inertia at the robot's end-effector through, for instance, an impedance control). Now, the set point of the manipulator is in a region around point 2. When the first manipulator stops, the path planner realises that the impact has been damped, increasing the controller gains (apparent high inertia). In addition, depending on the cubic object's angular velocity and the second manipulator's desired catch position, the path planner sets a new set point for the manipulator around point 3 in terms of the desired position and velocity. The manipulator decelerates to stop in a closed vicinity of that set point. As a result, the object begins a free movement to where the second manipulator expects it. In the next step, the first manipulator moves to a position around point 4 and waits until it gets a signal from the second manipulator indicating that it has touched the object. Then, the first manipulator goes toward point 5 along a trajectory that guarantees a collision-free movement. The first manipulator waits at point 5 to get a signal showing that the object has been thrown upward. Receiving that signal, the first manipulator goes to point 1 and waits for touching and catching the object again.

The sketched policy of the planner and controller's non-prehensile juggling manipulation holds almost the same for the bipedal locomotion. The only differences are in the reference points and the trajectory between points 4 and 5 (see Fig. 18(a) and (b)). In the case of biped locomotion, the reference points are defined in the robots coordinate system attached to the trunk. In contrast, the reference points are described in the ground coordinate system in the object manipulation case. As it can be seen in Fig. 18(a) and (b), the trajectory which each leg follows during the process with respect to the trunk is very similar to the trajectory which each manipulator follows during the manipulation process with respect to the base point.

5.1.2. Similarity between the phases of object juggling and biped robot with flat-feet running

In an overall view, we may divide the non-prehensile juggling manipulation primitive into four phases, namely: throwing the object, free-flight, catching, and stabilisation (Fig. 19). The same cycle can be imagined for a runner biped robot. We explain the running behaviour of the robot during a semi-cycle.

- Throwing phase. The bipedal robot running's first step is "throwing" the body, during which the first leg carries the body and prepares it to throw and pass to the second leg. With the aid of Fig. 20, we can say that this phase occurs between stages 1 and 3. Albeit the support leg throws the body in this phase with an appropriate acceleration, this acceleration stems from ground interaction force. We should assume that the leg has no slippage relative to the ground during the process of throwing. If any slippage occurs, we cannot forecast what will be happened to the robot, and then we cannot offer a suitable control strategy to get a favourite behaviour from the body. So we have to assume that there is enough friction between the support leg and ground to avoid slippage between them.

- Free-flight phase. The free-flight is the second phase of running. Based on Fig. 20, this phase starts from stage 3 and continues until the next catching phase occurs, i.e., stage 7. Ignoring the effect of air resistance, we can assume that the free-flight depends only on the location and acceleration of the body at the moment of the beginning of the flight, i.e., in stage 3. It is considered that if the robot's body has some angular velocity at the moment of the beginning of the flight, then its orientation would change until the next catching would occur in stage 7.

- Catching phase. It is the third phase of the running process. In Fig. 20, this stage is from stage 7 to stage 9. A catch occurs when the second leg impacts the ground and settles on a stable edge. This occurs in stage 7, and it is desirable that the least impact forces would be generated by the impact between the robot leg and ground. The catching phase goes on until the vertical velocity of the body is damped completely. In general, we should analyse the impact process before and after it. It is necessary to compute the normal and tangent forces applied at the impact point and calculate the slippage of the impacting vertex.

- Stabilisation phase. This stage enters into the computa-

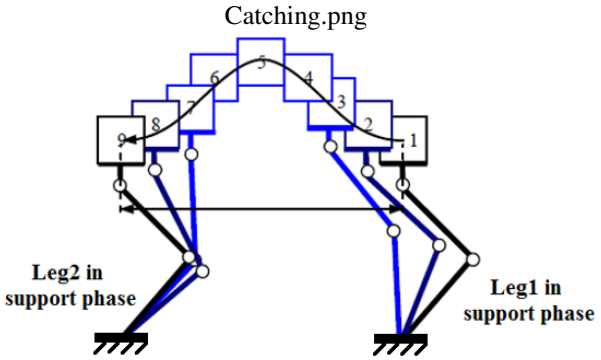

Figure 20: Stages (from 1 to 9) of the body movement during running.

tional cycle when the bipedal robots may be on the verge of instability for any reason and may fall.

5.1.3. Similarity between object juggling and walking

Figure 21 displays the snapshots of a polygonal object manipulation on an inclined surface using one-degree-of-freedom manipulators. Assume that the bases of the first, second, and third manipulators are installed in the positions P_a, P_b, and P_c, respectively. The object is first carried by the first manipulator, delivered to the second robot, and then to the third one. In this way, object manipulation is performed by a set of manipulators. The red triangle on one edge of the hexagon object illustrates the orientation of that edge during manipulation. The general impression is that the object is manipulated periodically and in the same manner by the manipulators.

In Fig. 22, the stick diagram of a two-link walker on the same inclined surface is demonstrated. In the position $\bar{P}_a$, one leg is in the support phase, and the other leg is in the swing phase. In the position $\bar{P}_b$, the status of the legs changes, and in $\bar{P}_c$ the status of the legs is reversed again. In Fig. 22, the red lines indicate the status of the support leg, and the blue lines indicate the status of the swing foot. It is observed that the walking process is executed periodically while maintaining the robot's stability.

Comparing the two Figs. 21 and 22, we find that the points $\bar{P}_a$, $\bar{P}_b$, and $\bar{P}_c$, which belongs to the support legs at different times, correspond to the base points P_a, P_b, and P_c, respectively. That is, the task of carrying the body of the two-link walker by the supporting leg is similar to the task of carrying the object by the corresponding manipulator. Also, it is observed that the trajectory of the two-link walker's body is similar to the trajectory of the manipulated object. In Fig. 21, if we assume that each manipulator is attached to the object and acts as the leg of two-link walker in the carrying phase of the object manipulation, we can reach this result that the two processes are very similar.

5.1.4. Similarity between stability criteria in biped locomotion and dynamic grasp criteria in juggling

Now, stability conditions for locomotion of flat-foot bipedal robots and dynamic grasp criteria in 2-dimensional juggling are discussed and compared.

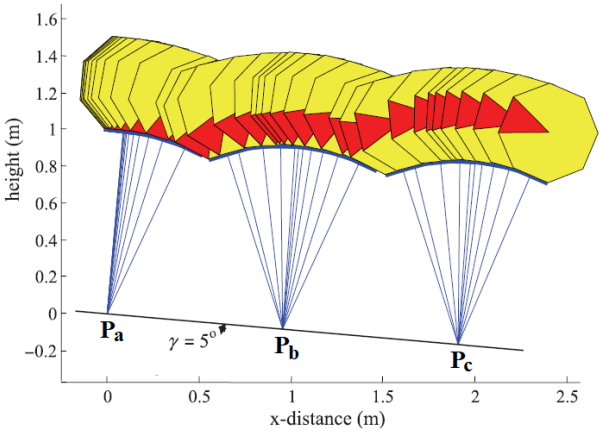

Figure 21: Snapshots of a polygonal object non-prehensile manipulation on a inclined surface. The red triangle on one edge of the hexagon illustrates the orientation of that edge (courtesy of Beigzadeh et al. (2013)).

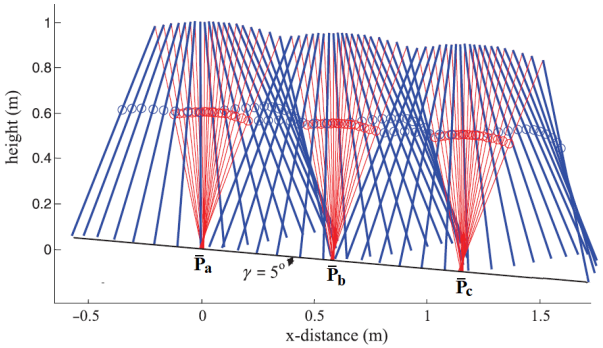

Figure 22: Snapshots of a gait of a two-link walker on a inclined surface. The red lines indicate the status of the support leg. The blue lines indicate the status of the swing foot (courtesy of Beigzadeh et al. (2013)).

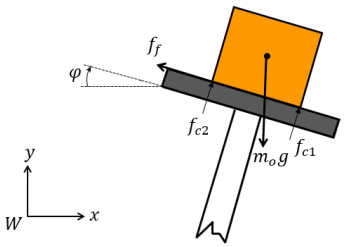

Figure 23: Forces applied to an object located on the palm of juggler robot.

- Stability criteria in biped locomotion. For a planar biped robot, we use the ZMP stability conditions (20) and (21) in $x-z$ coordinates as

$$x_{zmp,l} - x_{cog} \leq \frac{\dot{h}_y - M\ddot{x}_{cog} z_{cog}}{M(g + \ddot{z}_{cog})} \leq x_{zmp,u} - x_{cog}. \quad (25)$$

To keep the foot in contact with the ground, we should have $g + \ddot{z}_{cog} > 0$, as pointed out by Spong et al. (2007). Then, from (25), we have

$$M\ddot{x}_{cog} z_{cog} - M(x_{cog} - x_{zmp,l})(g + \ddot{z}_{cog}) - \dot{h}_y \leq 0, \quad (26)$$

$$-M\ddot{x}_{cog} z_{cog} + M(x_{cog} - x_{zmp,u})(g + \ddot{z}_{cog}) + \dot{h}_y \leq 0. \quad (27)$$

The friction constraint (24) must hold to get stable support. Besides, normal and tangential components of the contact force in the centre of pressure are $f_{f_z} = M(g + \ddot{z}_{cog})$ and $f_{f_x} = M\ddot{x}_{cog}$, as written by Sardain and Bessonnet (2004). Thus, from (24), we have

$$-\ddot{x}_{cog} - \mu_p(g + \ddot{z}_{cog}) < 0, \quad (28)$$

$$\ddot{x}_{cog} - \mu_p(g + \ddot{z}_{cog}) < 0. \quad (29)$$

Putting (26), (27), (28), and (28) together, we obtain the following foot stability conditions

$$\begin{bmatrix} Mz_{cog} & -M(x_{cog} - x_{zmp,l}) & -1 \\ -Mz_{cog} & M(x_{cog} - x_{zmp,u}) & 1 \\ -1 & -\mu_p & 0 \\ 1 & -\mu_p & 0 \end{bmatrix} \begin{bmatrix} \ddot{x}_{cog} \\ g + \ddot{z}_{cog} \\ \dot{h}_y \end{bmatrix} \leq 0_4. \quad (30)$$

The four inequalities in (30) are sufficient conditions for robot stability.

- Dynamic grasp criteria in juggling. Consider the case that a square object of length $d > 0$ is settled on the palm of a juggler robot as shown in Fig. 23. In this figure, the normal force to the palm is decomposed into two forces, $f_{c1} \in \mathbb{R}^2$ and $f_{c2} \in \mathbb{R}^2$, applied to the vertices of objects resting edge, and $f_f \in \mathbb{R}^2$ is the friction force. The following equations hold at any time

$$\begin{cases} f_{c1}\sin(\varphi) + f_{c2}\sin(\varphi) - f_f\cos(\varphi) = m_o\ddot{x}_G, \\ f_{c1}\cos(\varphi) + f_{c2}\cos(\varphi) + F_f\sin(\varphi) - m_o g = m_o\ddot{y}_G, \\ f_{c1}d - f_{c2}d - f_f d = \dot{h}_G, \end{cases} \quad (31)$$

where $x_G, y_G \in \mathbb{R}^2$ are the coordinates of the objects CoM expressed in the world frame W, $\dot{h}_G$ is the objects angular momentum about its CoM, $m_o >$ is the object mass, $\varphi \in \mathbb{R}$ is the angle of the palm with respect to the horizontal axis of W, and $g \in \mathbb{R}^2$ is the gravity vector. For the sake of comparison with the stability condition in biped locomotion, we assume a horizontal palm during the manipulation (i.e., $\varphi = 0$). Then, we have

$$\begin{cases} -f_f = m_o\ddot{x}_G, \\ f_{c1} + f_{c2} - m_o g = m_o\ddot{y}_G, \\ f_{c1}d - f_{c2}d - f_f d = \dot{h}_G. \end{cases} \quad (32)$$

To retain dynamic grasp while transporting the object, we should have

$$\begin{cases} f_{c1} > 0, \\ f_{c2} > 0, \\ |f_f| < \mu|f_{c1} + f_{c2}|, \end{cases} \quad (33)$$

with $\mu > 0$ the friction coefficient. Finding f_{c1}, f_{c2}, and f_f from (32), replacing them into (33) yields

$$\begin{bmatrix} m_o d/\sqrt{2} & -m_o d/\sqrt{2} & -1 \\ -m_o d/\sqrt{2} & -m_o d/\sqrt{2} & 1 \\ -1 & -\mu & 0 \\ 1 & -\mu & 0 \end{bmatrix} \begin{bmatrix} \ddot{x}_G \\ g + \ddot{z}_G \\ \dot{h}_G \end{bmatrix} \leq 0_4. \quad (34)$$

If (x_l, y_l) and (x_r, y_r) are coordinates of the resting edges left and right vertices in W, we have $x_l = x_G - d/\sqrt{2}$, $y_l = y_G - d/\sqrt{2}$, $x_r = x_G + d/\sqrt{2}$, and $y_r = y_G - d/\sqrt{2}$. Substituting these parameters into (34) yields

$$\begin{bmatrix} -m_o d(y_l - y_G) & m_o d(x_l - x_G) & -1 \\ m_o d(y_r - y_G) & -m_o d(x_r - x_G) & 1 \\ -1 & -\mu & 0 \\ 1 & -\mu & 0 \end{bmatrix} \begin{bmatrix} \ddot{x}_G \\ g + \ddot{z}_G \\ \dot{h}_G \end{bmatrix} \leq 0_4. \quad (35)$$

The four inequalities (35) are sufficient conditions for dynamic grasp.

In the above two robotic systems (juggler system and biped robot), we assume that enough friction exists between the object and the palm, and between the biped robot's feet and the ground, to prevent object and feet sliding, respectively. Comparing (30) with (35), we conclude that the stability conditions in support phases of biped robot and dynamic grasp conditions during the transporting phase of a juggling task have the same structure. In (30) and (35), if the condition related to the first row is violated, the heel acts as a pivot so that the foot turns about it, while the left vertex of the support edge will act as a pivot and the object rotates about it, respectively. If the condition related to the second row is violated, the toe acts as a pivot so that the foot rotates about it, while he right vertex of the support edge acts as a pivot and the object rotates about it, respectively. If both the first and second lines are violated, the foot leaves the ground, while the object leaves the palm, respectively.

5.1.5. *Throwing model in juggling manipulation and biped locomotion*

The throwing motion is generated subject to several constraints. Common constraints are listed below.

(a) Joint variable limits.

$$q_i^L \leq q_i \leq q_i^U, \tag{36}$$

where $q_i^L \in \mathbb{R}$ and $q_i^U \in \mathbb{R}$ are the lower and upper bounds for the joint $q_i \in \mathbb{R}$.

(b) Actuator torque capacities.

$$\tau_i^L \leq \tau_i \leq \tau_i^U, \tag{37}$$

where $\tau_i^L \in \mathbb{R}$ and $\tau_i^U \in \mathbb{R}$ are the lower and upper bounds for the joint torque $\tau_i \in \mathbb{R}$.

(c) Feet positions and orientations. The global coordinates and the angles about the global z_0 axis for both feet are assigned for each phase.

(d) Dynamic balance. The ZMP should exist within the foot support region (FSR), a convex hull (excluding the boundaries) generated by the surfaces of the contacting foot. The FSR is simply the single foot contact area for the single support phase. For the double support phases, the FSR is formed by the contact areas of both feet (Fig. 13).

(e) Time boundary conditions.

$$q_i(t^{release}) = q_i^{release},\ \dot{q}_i(t^{release}) = \dot{q}_i^{release},\ \ddot{q}(t^{release}) > 0, \tag{38}$$

where $q_i^{release} \in \mathbb{R}$ and $\dot{q}_i^{release} \in \mathbb{R}$ are the value of i-th joint position and velocity when the support leg is released or detached from the ground.

(f) Leg release orientation. For a flat ground, the orientation angle is formed between the support foot and the body's CoM.

(g) Target distance throw. The body of the biped robot is required to reach a given target point, the release position, release velocity, and flight time must satisfy the projectile equation.

For the non-prehensile juggling primitive, the constraints (a) and (b) are the same. Instead, "palm position and orientation" must be used in (c). The term "Dynamic balance" condition (30) is replaced with "dynamic grasp" condition (35) in (d), which, as noticed in the previous subsection, have the same structure. For all the joints of the juggler robot, we will have time boundary conditions such as (38). Besides the palm orientation, we need to specify the orientation of the juggler's arm to achieve a better throw. Finally, when the thrown object is required to reach a given target point, the release position, release velocity, and flight time must satisfy the projectile equation.

Therefore, for both biped locomotion and juggling action, the throwing problem has an input vector, u consists of joint trajectory parameters, under the equality constraints h_T, and inequality constraints conditions h_M, in which the squared norm of the actuator torque vector is minimized. The output of this problem is the trajectory parameters of the object and the active body of the bipedal robot. The throwing model is shown in Fig. 24.

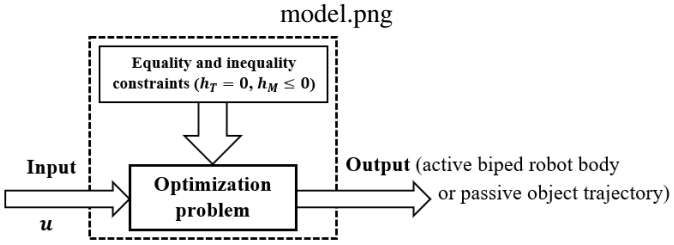

Figure 24: Schematic representation of the throwing model.

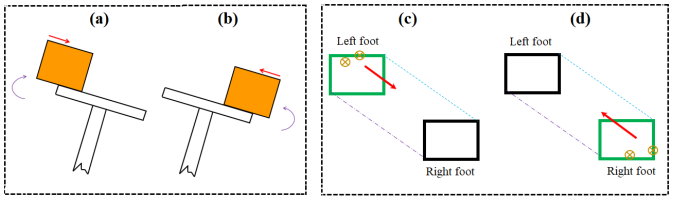

Figure 25: Similarity between non-full grasping ((a) and (b)) and marginal ZMP stability ((c) and (d)).

5.1.6. *Similarity between non-full grasping in juggling and marginal ZMP stability*

Balancing is more noticeable in fingerless jugglers. In jugglers with fingers, balancing is conceivable in the form of grasping. That is, grasping objects with the fingers prepares the object to be thrown in the right direction. So, the balancing stage can be called the grasping stage in jugglers with fingers.

In juggling actions with polygon objects such as cubic/rectangle objects, during the caching phase, the object may not completely lie on the palm (end-effector surface) of the juggler robot, and part of it may go out of the palm. This is called non-full grasping (Fig. 25(a)-(b)). Suppose the juggler does not react quickly and does not make the necessary corrections for full grasping. In that case, the object may be out of the throwing manipulation, or the robot may not throw the object correctly towards the target. As shown in Fig. 25(a)-(b), the object should be moved towards the centre of the palm.

In the case of a bipedal robot, consider a situation in which the gait of the robot is disturbed, and the robot's ZMP goes to the corners of the leg to be removed in the next cycle (Fig. 25(c)-(d)). In this case, the robot must make corrective actions before moving the support leg, that is, move ZMP towards the other leg (as in Fig. 25(c)-(d)). Otherwise, the robot may become unstable and fall.

Therefore, the stabilisation phase is needed in both object juggling and biped locomotion.

5.1.7. *Similarity between catching in juggling and touch down in locomotion*

A catch occurs when the object impacts the juggler's palm and settles to a stable edge. To achieve a steady catch, the impact magnitude at the catch time should be reduced. The catching task is complex since it consists of many impacts. To simplify the analysis, we assume that friction at the impact point is sufficiently high and the restitution coefficient low enough that the post-impact velocity of the impact point on the object is zero. Under these assumptions, which consider the impact as "sticking", the object quickly settles to rest, reducing throw-catch cycle time (Lynch et al. (2001)). If such a sticking impact occurs, assuming changes in joint angles of the object at impact time to be negligible, pre-impact relative velocity $(v^-_{x\_impact}, v^-_{y\_impact}, \omega^-_{impact})$ and post-impact relative velocity $(v^+_{x\_impact}, v^+_{y\_impact}, \omega^+_{impact})$ of the objects CoM and the palm will satisfy (Lynch et al. (2001))

$$v^+_{x\_impact} - y_{impact}\omega^+_{impact} = 0, \tag{39}$$

$$v^+_{y\_impact} - x_{impact}\omega^+_{impact} = 0, \tag{40}$$

$$m_o x_{impact}(v^+_{y\_impact} - v^-_{y\_impact}) - m_o y_{impact}(v^+_{x\_impact} - v^-_{x\_impact}) = I_{impact}(\omega^+_{impact} - \omega^-_{impact}), \tag{41}$$

where $I_{impact} > 0$ is the total inertia of the object at the impact time and (x_{impact}, y_{impact}) is a vector from the object's CoM to the impacting vertex. Equations (39) and (40) imply zero velocity of the impact vertex, whereas (41) ensures that the impulse force passes through the contact point. The post-impact angular velocity about the contact point (ω^+_{impact}) can be easily calculated through (39)–(41). To achieve a sticking impact, the impact force should be reduced and/or it should be absorbed. To this end, it is possible to perform a compliance control in the joints of the manipulator and the object at the impact time. It is also possible to create physical compliance by covering the palm and the sole surfaces with a high-friction and low-restitution fabric (Lynch et al. (2001)). Under these solutions, the impact is absorbed, and the impulsive force exerted to the foot is small, and a sticking impact will occur.

In the case of locomotion, the leg of the biped robot should land on the heel or toe, and then it should settle on the sole. This limits the angular release velocity to small values, which yields low speeds at the catching time.

5.2. *Connection between juggling motions with impact and the locomotion of point-foot legged robots*

In this subsection, we assume that a maximum of one robot leg is used as a support leg at any given time. Similar to the previous subsections, the similitude between juggling motions with impact and the locomotion of point-foot legged robots are summarised below.

1. Consider some snapshots of a real human running illustrated in Fig. 26. In Fig. 27, the time diagram is given.

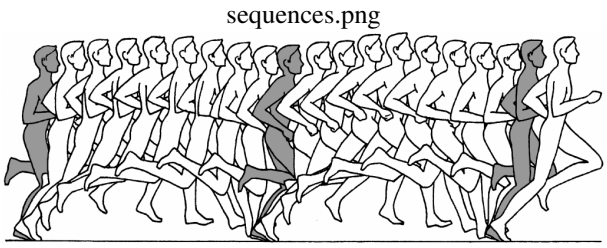

Figure 26: Snapshots from a real human running.

According to this last, $T_{ri} > 0$ and $T_{li} > 0$ are the time instants when the right and left legs hit the ground, and $T_{ff} > 0$ is related to the free-flight phase in which the feet have no contact with the ground. Therefore, T_{ri} and T_{li} are called impact times. These impact times will become smaller with increasing the running speed. So, the running includes two phases: the impact phase and the free-flight phase, that are iterated as shown in Fig. 28. On the other hand, in ball-juggling robots in Section 3, we have observed that the ball is in free-flight motion, and its dynamic behaviour is controlled by the force impact at the impact times. Also, we have analysed the dynamic behaviour of inverse and normal pendulum subject to impact effect. We inferred that the pendulum's motion under impact is confined to the desired region. Therefore, the juggler robots and mechanical systems with impacts have the same iterative cyclic activity shown in Fig. 28.

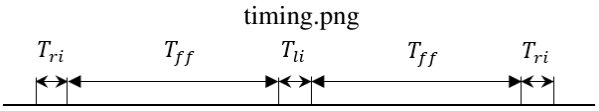

Figure 27: Real human running timing diagram.

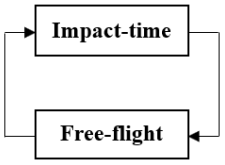

Figure 28: Iterative object juggling and biped robot running sequences.

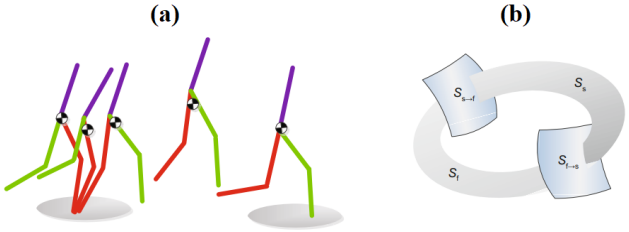

Figure 29: (a) Visualisation of biped running step, and (b) state sets of a biped running and juggler system (courtesy of Yi and Lin (2015)).

2. The running motion consists of support and flight phases with instantaneous takeoff and touchdown transitions

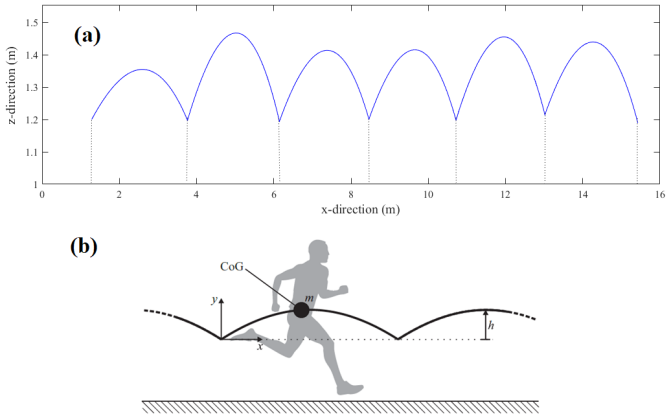

Figure 30: (a) The behaviour of the states of ball motion during several cycles, and (b) the idealised path of a runner's CoM position.

(Fig. 29(a)). Let S_s and S_f be the sets of valid states in the stance phase and flight phase, respectively, and let $S_{s\to f}$ and $S_{f\to s}$ be the sets of valid states at takeoff and touchdown, respectively. A visualisation of a running step is given in Fig. 29(b). This statement is also true for ball-playing juggler robots. Because the ball and juggler robots are in free-flight phase or in impact phase, and the state sets of juggler systems will be as Fig. 29(b).

3. In the high-speed running motion of bipedal robots, the movement patterns of the robot body are similar to the ball motion. To compare the behaviour of the bipedal robot body in a running scenario with a juggling system, the behaviour of a ball during several cycles in a juggling system and the idealised path of a runner's CoM position are illustrated in Fig. 30(a) and (b). We observe that the runners centre of mass position behaviour is very similar to the behaviour of the states of the juggling system. The overall assessment is that the catching time of the juggling systems is minimal, and also, since the object's mass is negligible, the object is thrown to a higher altitude in a bit of time.

4. Farid and Ruggiero (2022) found out that two phases can be recognzied in a ball-playing juggler system: a free-motion or impact-less phase and an impact phase. Therefore, the dynamic equations of two ball-playing juggler robot can be written in the general form of a nonlinear Lagrangian hybrid system as follows

$$\begin{cases} M(q)\ddot{q} + C(q,\dot{q})\dot{q} + g_0(q) = B\tau, & \vartheta(q) \neq 0 \\ q^+ = \Delta_n(q)q^-, & \vartheta(q) = 0 \\ \dot{q}^+ = \Delta_s(q,\dot{q})\dot{q}^-, & \vartheta(q) = 0 \end{cases} \tag{42}$$

where $\Delta_n(q) \in \mathbb{R}^{n\times n}$ and $\Delta_s(q) \in \mathbb{R}^{n\times n}$ are called the position renaming and velocity resetting matrices. Besides, $\vartheta(q) = 0$ is a state-dependent impact condition, the apexes $+$ and $-$ denote the quantities at a time instant after and before the impact, respectively. Considering the structure of the juggler robots in Fig. 6, the juggler dynamic in (5), the ball dynamics in (11) and its velocity resetting condition in (12) and (13), q, M, C, g_0, B, τ, Δ_n, and Δ_s in (42) take the following values

$$q = \begin{bmatrix} p_b^T & q_{J1}^T & q_{J2}^T \end{bmatrix}^T,$$

$$\dot{q} = \begin{bmatrix} v_b^T & \dot{q}_{J1}^T & \dot{q}_{J2}^T \end{bmatrix}^T,$$

$$M = \text{blockdiag}\Big(m_b I_3, M_{J1}(q_{J1}), M_{J2}(q_{J2})\Big)$$

$$C = \text{blockdiag}\Big((-\frac{1}{2}\rho s_a c_a \|v_b\| + \rho\omega_b r_b s_a c_l) I_3, C_{J1}(q_{J1}), C_{J_2}(q_{J_2})\Big)$$

$$g_0 = \begin{bmatrix} 0 & 0 & -m_b g & G_{J1}^T(q_{J1}) & G_{J2}^T(q_{J1}) \end{bmatrix}^T,$$

$$\tau = \begin{bmatrix} \tau_{J1}^T & \tau_{J2}^T \end{bmatrix}^T,$$

$$B = \begin{bmatrix} 0_{3\times 2m}^T & B_{J1}^T & B_{J2}^T \end{bmatrix}^T,$$

$$\Delta_n = I_9,$$

$$\Delta_s = \text{diag}\Big(\text{diag}(v_{b_x}^+, v_{b_y}^+, v_{b_z}^+), I_3, I_3\Big),$$

with $I_\times$ the identity matrix of proper dimensions. For a three-degree-of-freedom juggling system, the impact condition was given in (6).

Also, Farid and Ruggiero (2021) showed that in case, at any given time, one leg of biped robot is in contact with the ground and the other leg is in swing phase and, at time instant $t = t_k$, the status of the foots change, the dynamic equations of a biped robot can be written in the same form of a nonlinear Lagrangian hybrid system given by (42). For a typical two-link walker, from Fig. 31, the switching condition can be written as

$$\vartheta(q) = h_1(q) + h_2(q) - h_\phi(q) = 0 \tag{43}$$

where

$$h_1(q) = l\cos(-q_1) \tag{44}$$

$$h_2(q) = l\cos(q_2) \tag{45}$$

$$h_\phi(q) = L\tan(\phi) \tag{46}$$

$$L = l\sin(-q_1) + l\sin(q_2) \tag{47}$$

where $l = a + b$. Therefore, ball-playing juggler systems and point foot biped robots have the single-mode hybrid model as shown in Fig. 15. From the controller design viewpoint, since the dynamic equation of biped robot and juggler system are in the same form, each effective controller designed for juggler systems applies to the biped robots.

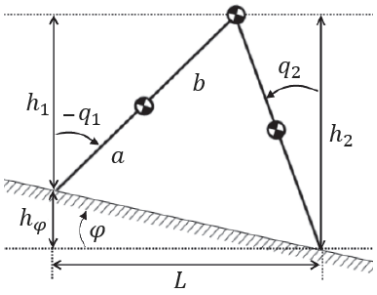

Figure 31: Illustration showing the different quantities used when defining the impact surface of the biped.

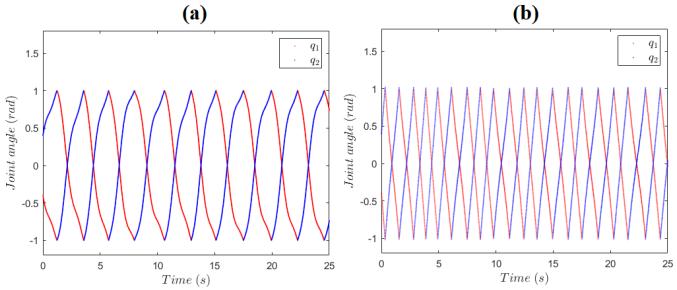

Figure 32: Decomposition of the outputs normal pendulum (a) and inverse pendulum into q_1 and q_2.

5. In ball-playing juggling actions, the object's motion is controlled by the impact-like forces applied at impact times. The stability and the speed of bipedal robots in high-speed running motions are governed by the reaction ground forces inserted by the legs to the ground. These forces are in the form of impulse forces and have a short life, and determine the speed of the bipedal robots after the robot hits the ground. The value of these forces depend on the pre-impact and post-impact joint rates of these robotic systems and also the value of the mass and inertia matrix after impact

$$\delta F = M(q(t_k^+))\dot{q}(t_k^+) - M(q(t_k^-))\dot{q}(t_k^-). \qquad (48)$$

6. The dynamic behaviour of two-link compass-like biped robot in walking condition introduced by Farid and Ruggiero (2021) is similar to two impacting pendulums presented in Section 3.1. Therefore, the output angle ϕ can be used as a reference trajectory for the two-link walker. As shown in Fig. 32, we have decomposed the angle ϕ in two q_1 and q_2 as reference trajectories for the two-link walker.

7. A type of high-speed "jogging in place exercise" is very similar to the juggling action of two juggler robots. As shown in Fig. 33, at the initial time t_0, a biped robot is in its initial standing status (Fig. 41(a)), and the sequences of Figs. (b)→(c)→(d)→(c)→(b) are related to joggling in place exercise. In this exercise, the biped robot controls its dynamic stability by inserting impacts to the ground. The hybrid model of this robot will be as a double-mode hybrid model (Fig. 16), in which the robot is in free-flight

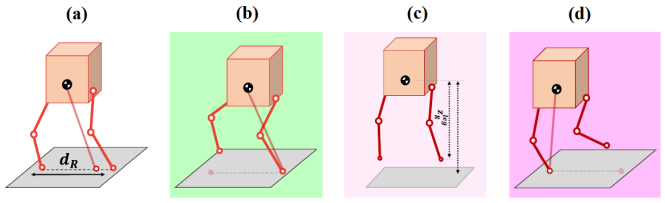

Figure 33: (a) Initial standing status of a typical biped robot, and the sequences of (b)→(c)→(d)→(c)→(b) are related to joggling in place exercise.

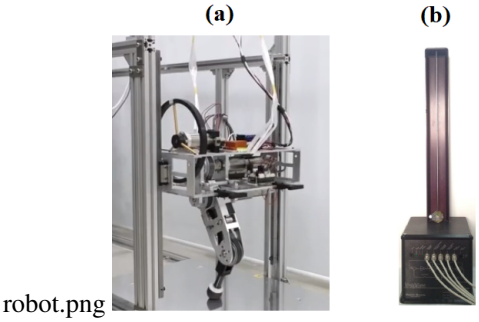

Figure 34: (a) Typical hopping robot, and (b) the geometrical structure of a juggler system consisting of a bouncing ball, an actuated piston, and a vertical rod (courtesy of Tian et al. (2013)).

or contact with the ground, and the joint velocities after impacts are updated according to the previous values of joint velocities before impact.

8. The dynamic behaviour of confined hopping robot in vertical plane (Fig. 34(a)) is similar to the dynamic behaviour of juggler system (Tian et al. (2013)) shown in Fig. 34(b). The main difference is that a hopping robot is an active object with a high mass, and it needs a larger force to overcome the friction of its movement environment.

9. The quadruped robots' running (bounce) gait patterns are similar to the juggler robot motions and high-speed locomotion of biped robots. The running cycle is shown in Fig. 35. This cycle can be transformed into the cycle shown in Fig. 28, because we have two impact phases and two free-flight phases, which are repeated in a cycle.

10. When four-legged animals walk in trot and pace gait patterns, they should quickly change the position of the legs diagonally or symmetrically to maintain dynamic stability. This type of movement of the quadruped robots is similar to the movement of two-legged robots with high-speed locomotion, in which at any moment, there is only one foot on the ground as a support foot. When feet collide with the ground, the dynamics of the quadruped robots change. In

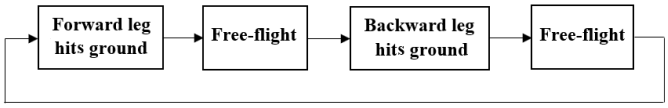

Figure 35: Quadruped running sequence in a bounce gait.

this case, the motion dynamics of the quadruped robots can be demonstrated as a switching system shown in Fig. 15.

6. Stabilisation of mechanical systems with hybrid dynamics

In this section, a general control framework with finite-time stability property is proposed for the introduced hybrid Lagrangian systems (42), which can be applied to both classes of non-prehensile juggler systems and biped robots. The control method is designed based on zero dynamics and the integral sliding mode approach. The centralised controller must drive the output function of the system to zero in finite time.

6.1. Zero dynamic based integral sliding mode controller design

The continuous part of the hybrid system (42) can be written as

$$\ddot{q} = f(q, \dot{q}) + \eta(q)u, \tag{49}$$

where $f(q, \dot{q}) = -M^{-1}(q)(C(q, \dot{q}) + g_0(q))$, $\eta(q) = M^{-1}(q)$, and $u = B\tau$. For systems (49), let $q \in P$ be a set of generalised coordinates. The output of the system (49) is defined as

$$y = h(q) = q - h_d(\theta), \tag{50}$$

where $h_d(\theta) \in \mathbb{R}^n$ is the desired trajectory vector and $\theta \in \mathbb{R}^{n_\theta}$ is the parameter vector of the desired trajectory. Adding the velocities $\dot{q} \in Q$ to the configuration variables gives the zero dynamics manifold as

$$\mathcal{Z} = \left\{(q, \dot{q}) \in PQ \;\middle|\; y = h(q) = 0_n,\ \dot{y} = \frac{\partial h}{\partial q}\dot{q} = 0_n\right\}. \tag{51}$$

By using the standard Lie derivative notation (Westervelt et al. (2007)), direct calculation produces the following relations

$$\frac{d}{dt}\begin{bmatrix} y \\ \dot{y} \end{bmatrix} = \begin{bmatrix} \dot{h}(q) \\ L_f^2 h(q) \end{bmatrix} + \begin{bmatrix} 0_n \\ L_\eta L_f h(q) \end{bmatrix} u, \tag{52}$$

where

$$\dot{h}(q) = L_f h(q) + L_\eta h(q) u, \tag{53}$$

$$L_\eta h(q) = 0_n. \tag{54}$$

Define $e_x = h(q) \in \mathbb{R}^n$ and $e_v = \dot{h}(q, \dot{q}) \in \mathbb{R}^n$. Furthermore, define an integral sliding surface as

$$s = e_v + \int_0^t \left(K_{e_v}[e_v]^\alpha + K_{e_x}[e_x]^\beta\right) dr, \tag{55}$$

where $K_{e_x} \in \mathbb{R}^{n\times n}$ and $K_{e_v} \in \mathbb{R}^{n\times n}$ are two positive definite diagonal matrices, $0 < \alpha, \beta \leq 1$, and $[e_v]^\alpha = \text{blockdiag}\left(|e_{v_1}|^\alpha, ..., |e_{v_n}|^\alpha\right)\text{sign}(e_v)$.

Theorem 1. *For the sliding surface* (55) *and in sliding-mode condition, the output* $y = h(q)$ *and its time derivative become zero. The introduced zero dynamic manifold* (51) *can be thus obtained.*

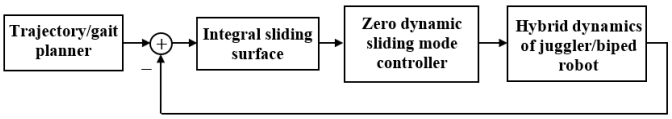

Figure 36: The devised control system for mechanical systems with hybrid dynamics.

Proof. When the controller puts the system into the sliding mode (i.e., $s(t) = 0_n$), from the sliding dynamics $\dot{s}(t) = 0_n$, the following result can be extracted

$$\begin{cases} \dot{e}_x = e_v, \\ \dot{e}_v = -K_{e_v}[e_v]^\alpha - K_{e_x}[e_x]^\beta. \end{cases} \tag{56}$$

Consider the Lyapunov function candidate as

$$V_e = \frac{1}{2}e_v^T e_v + \frac{1}{\beta+1}\sum_{i=1}^{n} k_{e_{x_i}}|e_{x_i}|^{\beta+1}. \tag{57}$$

Taking its time derivative along the sliding dynamics (56) yields

$$\begin{aligned} \dot{V}_e &= -e_v^T K_{e_v}[e_v]^\alpha - e_v^T K_{e_x}[e_x]^\beta + \sum_{i=1}^{n} \dot{e}_{x_i} k_{e_{x_i}} \text{sign}(e_{x_i})|e_{x_i}|^\beta \\ &= -e_v^T K_{e_v}[e_v]^\alpha \leq -2^{\frac{\alpha+1}{2}} \lambda_{min}(K_{e_v}) V_e^{\frac{\alpha+1}{2}}. \end{aligned} \tag{58}$$

In (58), when $t \to \left(t_0 + \dfrac{V^{\frac{1-\alpha}{2}}(t_0)}{2^{\frac{\alpha-1}{2}}\lambda_{min}(K_{e_v})(1-\alpha)}\right)$, then $e_v \to 0_n$. This means that the velocity tracking error converges to the origin in a finite time. Substituting $e_v = 0$ in (56) gives

$$\begin{cases} \dot{e}_x = 0_n, \\ \dot{e}_v = -K_{e_x}[e_x]^\beta. \end{cases} \tag{59}$$

Assume that e_x converges to a nonzero constant vector. Then, from (59), we have $\dot{e}_v \neq 0_n$. In this case, e_v deviates from the origin and this assumption contradicts the obtained result. Therefore, finite time convergence property of e_x leads the convergence of e_v to the origin in a finite time. □

Time differentiating (55) and using (52) yield the following sliding surface dynamic

$$\begin{aligned} \dot{s} =& \ddot{y} + K_{e_v}[\dot{y}]^\alpha + K_{e_x}[y]^\beta = L_f^2 h(q) - \ddot{h}_d(\theta) + L_\eta L_f h(q) u \\ &+ K_{e_v}[L_f h(q) - \dot{h}_d(\theta)]^\alpha + K_{e_x}[h(q)]^\beta. \end{aligned} \tag{60}$$

The proposed robust integral sliding mode control law has the following structure

$$\begin{aligned} u = \left(L_\eta L_f h(q)\right)^{-1}\Big[&\ddot{h}_d(\theta) - L_f^2 h(q) - K_{e_v}[L_f h(q) - \dot{h}_d(\theta)]^\alpha \\ &- K_{e_x}[h(q)]^\beta\Big] - K_s \text{sign}(s), \end{aligned} \tag{61}$$

where $K_s \in \mathbb{R}^{n\times n}$ is a positive definite matrix. The block diagram of the closed-loop system containing the proposed control

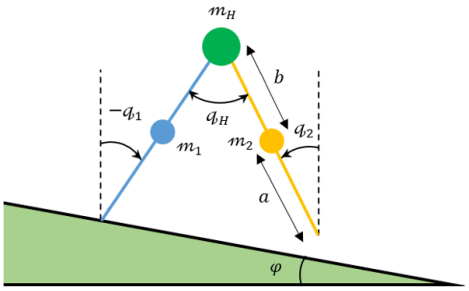

Figure 37: Schematic representation of a two-link walker on an inclined surface with slope $\phi > 0$.

is illustrated in Fig. 36. Note that, before applying the input-output linearization-based control law (61) to any Lagrangian system, its relative degree should be checked first, and the term $L_\eta L_f h(q)$ should be invertible. Under this condition, the control law (61) is realizable for that application.

Theorem 2. *Consider the dynamic of the sliding surface* (60)*, the proposed centralised control law* (61)*, and the results of Theorem 1, in which the zero dynamic manifold can be obtained under the sliding mode condition and with finite-time convergence property. If there exist two $\mathcal{K}$-class functions ω_1 and ω_2, some constants $\mu \in (0,1)$, $\rho > 0$, and $\kappa \in (0,1)$, and a locally Lipschitz continuous function $V(s)$, such that*

$$\omega_1(\|s\|) \leq V(s) \leq \omega_2(\|s\|), \tag{62}$$

$$V(s^+) \leq \mu V(s), \tag{63}$$

$$\dot{V}(s) \leq -\phi V^\kappa(s), \quad t \neq t_n, \tag{64}$$

then, the system (42) *is finite-time stable under any impact sequences.*

Proof. Substituting the control law (61) into (60) yields

$$\dot{s} = -K_s \text{sign}(s). \tag{65}$$

Select the following Lyapunov function candidate

$$V(s) = \frac{1}{2} s^T s. \tag{66}$$

Differentiating (66) along the sliding surface dynamic (65) yields

$$\dot{V} = -s^T K_s \text{sign}(s) \leq -\sqrt{2}\lambda_{min}(K_s) V^{0.5}. \tag{67}$$

Therefore, the system (42) without impact effects (49) is finite-time stable. The settling-time, depending on the initial state $s(0)$, is obtained by

$$t_s \leq \frac{\sqrt{2} V^{0.5}(s(0))}{\lambda_{min}(K_s)}. \tag{68}$$

Integrating both side of (67), from t_0 to t, yields

$$V^{0.5}(s) \leq V^{0.5}(s_0) - \sqrt{2}\lambda_{min}(K_s) t, \quad \forall t \in [t_0, t_s). \tag{69}$$

When $t_1 \geq t_s$, it indicates that the solution $s(t)$ is free of impulse. In this case, it is clear that $V(s(t)) \leq V(s_0)$, $\forall t \in [t_0, t_s]$, and $V(s(t)) = 0$ for all $t \geq t_s$ (Michel and Hu, 1999). When $t_1 < t_s$, assume that there are n impulsive points on the interval $[t_0, t_s]$, i.e., $t_0 < t_1 < ... < t_n < t_s$. Then, in view of $\mu \in (0,1)$, it is easy to derive that

$$V^{0.5}(s) \leq V^{0.5}(s_0) - \sqrt{2}\lambda_{min}(K_s) t, \quad \forall t \in [t_j, t_{j+1}), \tag{70}$$

for $j = 0, 1, ..., n$. It implies that $V(s(t)) \leq V(s_0)$, $V(s(t)) \leq V(s_0)$, $\forall t \in [t_0, t_s]$, and $V(s(t)) = 0$ for all $t \geq t_s$. For any $\epsilon > 0$, choose $\delta > 0$ such that $\omega_2(\delta) \leq \omega_1(\epsilon)$. Then, any s_0, $|s0| \leq \delta$ implies that $|s(t)| \leq \epsilon$ for $t \in [0, t_s]$, and $s(t) = 0$ for $t \geq t_s$. This indicates that the system (42) is finite-time stable when subjects to sequences of impacts. □

6.2. Simulation results

In this section, the efficiency of the proposed control algorithm will be evaluated with implementation on ball-playing juggler robots with three degrees of freedom (Fig. 6) and on a two-link walker.

The schematic structure of the employed two-link walker is shown in Fig. 37. The geometrical parameters and the details of the dynamic equations of the juggler robots and the two-link walker are given by Farid and Ruggiero (2022) and Farid and Ruggiero (2021), respectively. The sliding surface gains and control parameter are selected as $K_{e_v} = 2.5I_9$, $K_{e_x} = 12.5I_9$, $K_s = 2.5I_9$ (for the juggler robot) and $K_{e_v} = 5I_2$, $K_{e_x} = 25I_2$, $K_s = 5I_2$ (for the two-link walker). The closed-loop systems containing the dynamics of two robots, the proposed controller, trajectory/gait planner were implemented in MATLAB/Simulink. Differential equations were solved using the RungeKutta algorithm with a sampling time of 10^{-3} s.

Figures 38 and 39 show the profiles of the desired and measured angular positions of the joints. It can be observed that the measured angles track the desired trajectories precisely in a finite time. Figures 40 and 41 show that the ball-playing juggler systems and two-link biped robot have Zeno behaviours (Wendel and Ames (2010)), i.e., the position and velocity variables converge to the desired trajectories. Their phase-space has stable behaviours as their desired phase spaces. Control efforts of two robotic systems are plotted in Fig. 42 and Fig. 43. Notice that the control signals do not have any chattering-free and continuous behaviour, and only in impact times, spike-like signals with short amplitudes appear.

7. Conclusion

In this research work, the similarities between non-prehensile object manipulation and dynamic walking of biped robots have been discussed. In this direction, the basic concepts related to non-prehensile object manipulation, especially juggling tasks, the hybrid nature of juggler robot dynamics and biped robots, ZMP stability, and non-prehensile dynamic grasping conditions, were studied. Then, we proposed the duality of non-prehensile dynamic object manipulation and dynamic biped walking. We found that the behaviour of a two-link walker is

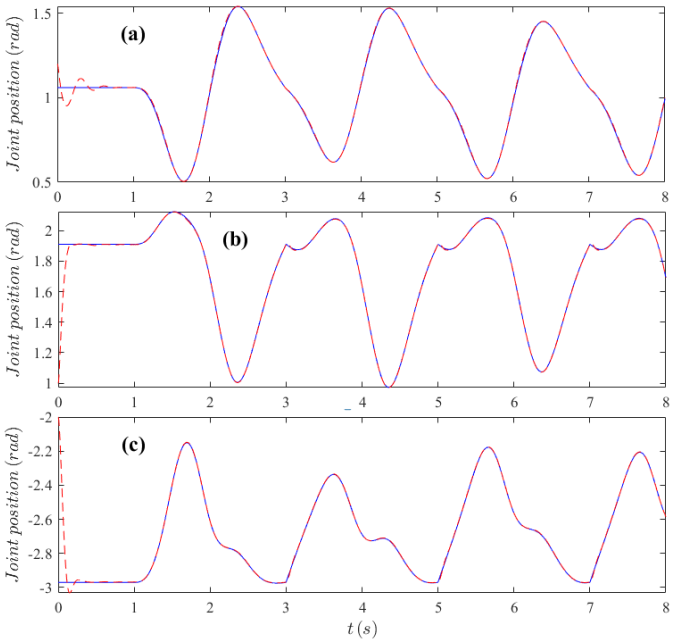

Figure 38: Desired, blue line, and measured, red dashed line, angular joint positions of the first juggler robot: (a) $h_{d_1}(\theta)$ and q_1, (b) $h_{d_2}(\theta)$ and q_2, and (c) $h_{d_3}(\theta)$ and q_3.

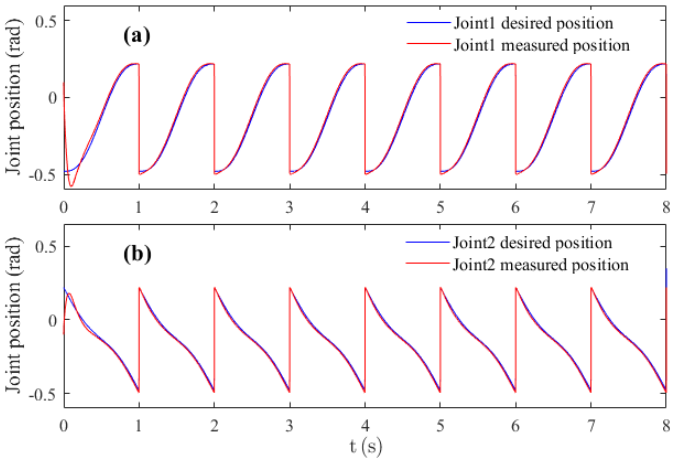

Figure 39: Desired, blue line, and measured, red line, joint angles of the two-link biped robot: (a) $h_{d_1}(\theta)$ and q_1, and (b) $h_{d_2}(\theta)$ and q_2.

very similar to the corresponding non-prehensile object manipulation system. Also, we extracted that the dynamic grasp in the catching phase of juggling systems and stability condition in the support phase of biped robots share similar sets of equations. Besides, we adapted a common throwing model for these systems. We exploited a unified control system framework for biped and juggler robots in terms of similarity of dynamic behaviour in impact conditions. After finding a general class of hybrid dynamic equations for juggler and biped robots, a common control framework based on zero dynamic concept and integral sliding mode approach was proposed. Simulation studies on walking control of the two-link walker and a three-degree-of-freedom ball-juggling robot proved that the proposed control

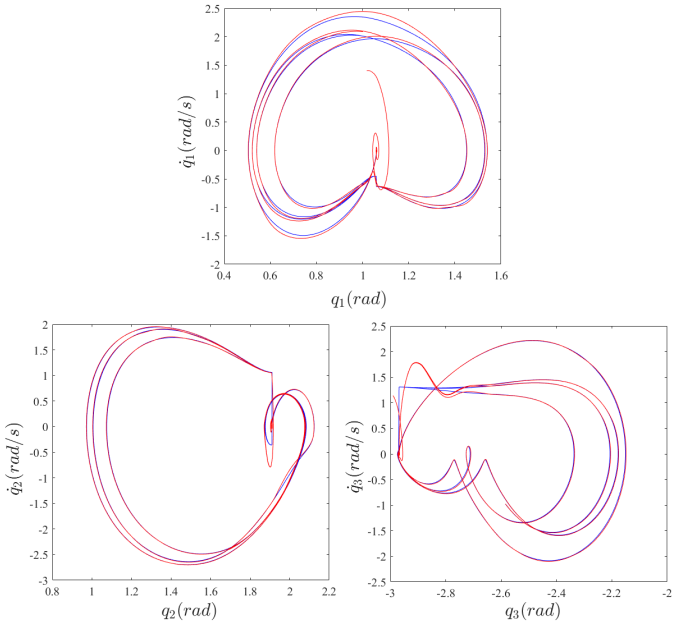

Figure 40: Phase portraits of the desired, blue line, and measured, red line, states of the first juggler robot.

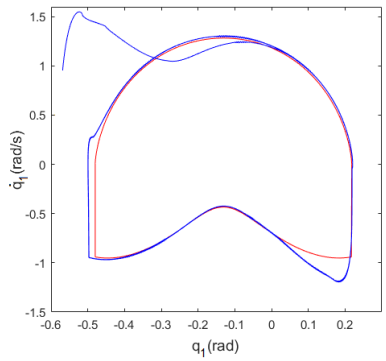

Figure 41: Phase portrait of $q_1 - \dot{q}_1$ for the two-link walker: the red line is the desired phase-space, while the blue line is the measured phase-space.

algorithm is efficient and can be implemented on real robots with hybrid dynamics.

In future work, we plan to focus on increasing the agility property of the point-foot biped robots in high-speed manoeuvres inspired by juggling actions with impact, such as table tennis playing robots. Then, new running stability criteria will be defined for the biped robots with hybrid dynamics. Also, the similarity of robust biped locomotion on unexplored terrain and two fingertips juggling an object with an unknown shape will be investigated. This case study will formulate three nonlinear optimization problems for catching, stabilization, and throwing phases. Dynamic uncertainty and unknown object dynamic and environment characteristics will be considered. Presenting high-speed (fast) solvers for these three optimization problems will be a significant challenge. Implementing the extracted algorithms on real juggler and biped robots will be part of our work. Besides, the juggling tasks can be performed at a wide range of speeds and impacts, which makes gathering

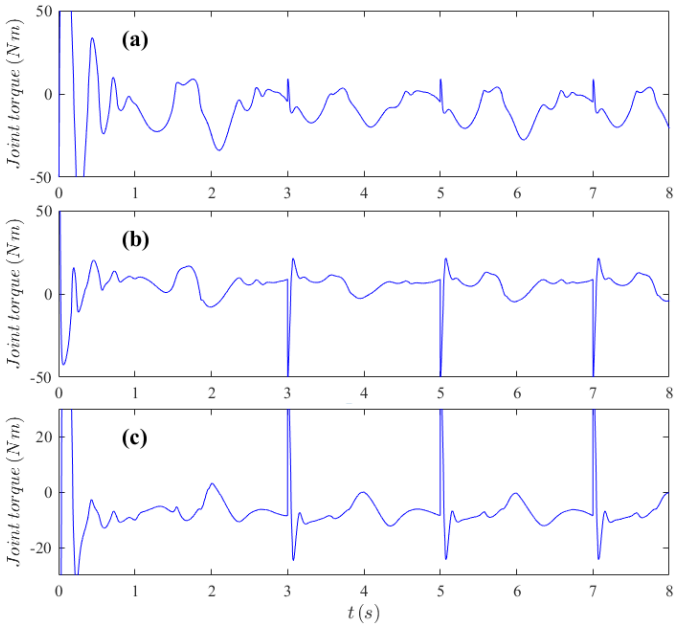

Figure 42: Control efforts of the joints of the first juggler robot: (a) τ_1, (b) τ_2, and (c) τ_3

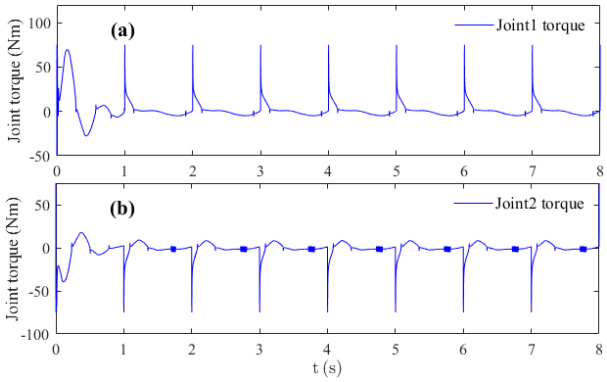

Figure 43: Control efforts of two-link walker: (a) τ_1, and (b) τ_2

a comprehensive set of experiences. For instance, this understanding could be very helpful in developing artificial learning algorithms for biped walking/running. Finally, more general approaches based on creating and in-turn stabilizing low-dimensional manifolds through orbital stabilization of systems with two and more passive degrees of freedom can be employed to explore further connections (Stre et al., 2021; Shiriaev and Freidovich, 2009).

Acknowledgment

The research leading to these results has been supported by both the PRINBOT project (in the frame of the PRIN 2017 research program, grant number 20172HHNK5_002) and the WELDON project (in the frame of Programme STAR, financially supported by UniNA and Compagnia di San Paolo). The authors are solely responsible for its content.

Abi-Farraj, F., Henze, B., Ott, C., Giordano, P., Roa, M., 2019. Torque-based balancing for a humanoid robot performing high-force interaction tasks. IEEE Robotics and Automation Letters 4, 2023–2030.

Akbarimajd, A., 2009. Optimal cyclic vertical juggling using 1-dof arm, proceedings of the 2009 ieee international conference on robotics and biomimetics, december 19 -23, 2009, guilin, china .

Akbarimajd, A., Ahmadabadi, M., Ijspeert, A., 2011. Analogy between juggling and hopping: active object manipulation approach. Advanced Robotics 25, 1793–1816.

Akella, S., Huang, W., Lynch, K., Mason, M.T., 2000. Parts feeding on a conveyor with a one joint robot. Algorithmica 26, 313344.

Ames, A.D., Galloway, K., Sreenath, K., Grizzle, J.W., 2014. Rapidly exponentially stabilizing control lyapunov functions and hybrid zero dynamics. IEEE Transactions on Automatic Control 59, 876–891.

Arcos-Legarda, J., Cortes-Romero, J., Tovar, A., 2019. Robust compound control of dynamic bipedal robots. Mechatronics 59, 154–167.

Arpenti, P., Donaire, A., Ruggiero, F., Lippiello, V., 2021. Energy pumping-and-damping for gait robustification of underactuated planar biped robots within the hybrid zero dynamics framework, pp. 415–421.

Asano, F., 2015. Fully analytical solution to discrete behavior of hybrid zero dynamics in limit cycle walking with constraint on impact posture. Multibody System Dynamics 35, 191–213.

Bae, H., Oh, J.H., 2018. Biped robot state estimation using compliant inverted pendulum model. Robotics and Autonomous Systems 108, 35–50.

Beigzadeh, B., Ahmadabadi, M., Meghdaria, A., Akbarimajd, A., 2008. A dynamic object manipulation approach to dynamic biped locomotion. Robotics and Autonomous Systems 56, 570–582.

Beigzadeh, B., Meghdari, A., Sohrabpour, S., 2013. Passive dynamic object manipulation: A framework for passive walking systems. Proceedings of the Institution of Mechanical Engineers, Part K: Journal of Multi-body Dynamics 227, 185–198.

Bicchi, A., Kumar, V., 2000. Robotic grasping and contact: A review, in: 2000 IEEE International Conference on Robotics and Automation.

Brogliato, B., 2016. Nonsmooth mechanics: models, dynamics, and control. Third edition, Springer International Publishing Switzerland.

Brogliato, B., Rio, A., 2000. On the control of complementary-slackness juggling mechanical systems. IEEE Transactions on Automatic Control 45, 235–246.

Buhler, M., Koditschek, D.E., Kindlmann, P.J., 1990. A family of robot control strategies for intermittent dynamical environments. IEEE Control Systems Magazine 10, 16–22.

Buhler, M., Koditschek, D.E., Kindlmann, P.J., 1994. Planning and control of a juggling robot. International Journal of Robotics Research 13, 101–118.

Chen, B.S., Tsai, Y.Y., Lee, M.Y., 2021. Robust decentralized formation tracking control for stochastic large-scale biped robot team system under external disturbance and communication requirements. IEEE Transactions on Control of Network Systems 8, 654–666.

Chevallereau, C., Abba, G., Aoustin, Y., Plestan, F., Westervelt, E.R., Canudas-de-Wit, C., Grizzle, J.W., 2003. Rabbit: A test bed for advanced control theory. IEEE Control Systems Magazine 23, 57–79.

Di Bernardo, M., Budd, C., Champneys, A., Kowalczyk, R., 2008. Piecewise-smooth dynamical systems. Theory and Applications. Springer-Verlag London Limited.

Duan, H., Dao, J., Green, K., Apgar, T., Fern, A., Hurst, J., 2021. Learning task space actions for bipedal locomotion, pp. 1276–1282.

Duindam, V., Stramigioli, S., 2009. Modeling and control for efficient bipedal walking robots. a port-based approach, in: Siciliano, B., Khatib, O., Groen, F. (Eds.), Springer Tracts in Advanced Robotics. Springer. volume 53.

Erumalla, S., 2018. Throwing, catching, and balancing of a disc with a disk-shaped end-effector by using a two-link manipulator. Department of Mechanical Engineering, Northern Illinois University .

Farid, Y., Ehsani-Seresht, A., 2021. Discrete finite-time robust fault-tolerant high-order sliding mode control of uncertain quadruped robot: an experimental assessment. International Journal of Intelligent Robotics and Applications 5, 23–36.

Farid, Y., Majd, V.J., Ehsani-Seresht, A., 2018. Observer-based robust adaptive force-position controller design for quadruped robots with actuator faults. International Journal of Adaptive Control and Signal Processing 32, 1453–1472.

Farid, Y., Majd, V.J., Ehsani-Seresht, A., 2021. Dynamic-free robust adaptive intelligent fault-tolerant controller design with prescribed performance for stable motion of quadruped robots. Adaptive Behavior 29, 233–252.

Farid, Y., Ruggiero, F., 2021. Finite-time disturbance reconstruction and robust fractional-order controller design for hybrid port-hamiltonian dynamics of biped robots. Robotics and Autonomous Systems 144, 103836.

Farid, Y., Ruggiero, F., 2022. Finite-time extended state observer and fractional-order sliding mode controller for impulsive hybrid port-hamiltonian systems with input delay and actuators saturation: Application to ball-juggler robots. Mechanism and Machine Theory 167, 104577.

Fevre, M., Goodwine, B., Schmiedeler, J.P., 2018. Design and experimental validation of a velocity decomposition-based controller for underactuated planar bipeds. IEEE Robotics and Automation Letters 3, 1896–1903.

Gim, K.G., Kim, J., Yamane, K., 2018. Design and fabrication of a bipedal robot using serial-parallel hybrid leg mechanism, pp. 5095–5100.

Goebel, R., Sanfelice, R., Teel, A., 2009. Hybrid dynamical systems. IEEE Control Systems Magazine 29, 28–93.

Goodwine, B., Burdick, J., 2000. Controllability of kinematic control systems on stratified configuration spaces. IEEE Trans. on Automatic Control 46, 58–368.

Gritli, H., 2019. Robust master-slave synchronization of chaos in a one-sided 1-dof impact mechanical oscillator subject to parametric uncertainties and disturbances. Mechanism and Machine Theory 142, 103610.

Grizzle, J.W., 2009. Mabel, a new robotic bipedal walker and runner, in: 2009 American Control Conference, pp. 2030–2036.

Grizzle, J.W., Chevallereau, C., Sinnet, R.W., Ames, A.D., 2014. Models, feedback control, and open problems of 3d bipedal robotic walking. Automatica 50, 1955–1988.

Guckenheimer, J., Holmes, P., 1983. Nonlinear oscillations, dynamical systems, and bifurcations of vector fields. Applied Mathematical Sciences 42.

Hamed, K.A., Ames, A.D., 2020. Nonholonomic hybrid zero dynamics for the stabilization of periodic orbits: Application to underactuated robotic walking. IEEE Transactions on Control Systems Technology 28, 2689–2696.

Horn, J.C., Mohammadi, A., Hamed, K.A., Gregg, R.D., 2020. Nonholonomic virtual constraint design for variable-incline bipedal robotic walking. IEEE Robotics and Automation Letters 5, 3691–3698.

IMG-1, . Pushing the car. https://www.istockphoto.com/nl/fotos/pushing-car.

IMG-2, . Pizza making. https://www.sciencephoto.com/media/208729/view/pizza-chef-holding-pizza-in-front-of-ove.

IMG-3, . Ball throwing. https://www.sportingnews.com/us/nba/news/kobe-bryant-most-memorable-games-nba-career/ygyczt2qz8rh1e2jarlsk49l6.

IMG-4, . Butterfly device. https://www.youtube.com/watch?v=V30e77x8BQA&t=163s.

IMG-5, . Batting task. https://en.wikipedia.org/wiki/Batting_(baseball).

IMG-6, . Juggling task. ttps://divineimpacts.wordpress.com/2013/01/27/juggling-through-life/.

IMG-7, . Car-juggling humanoid robot. https://www.theverge.com/2014/6/26/5846984/giant-robot-juggle-cars-bugjuggler.

IMG-ASIMO, . Asimo robot. https://asimo.honda.com/.

IMG-ATLAS, . Atlas robot. https://www.bostondynamics.com/atlas.

IMG-LOLA, . Lola robot. http://mindtrans.narod.ru/walkers/walkers.htm.

IMG-RuBi, . Rubi robot. https://ens-lab.sdu.dk/biped-robots/.

IMG-WABIAN, . Wabian-2r robot. http://www.takanishi.mech.waseda.ac.jp/top/research/wabian/.

Joe, H.M., Oh, J.H., 2018. Balance recovery through model predictive control based on capture point dynamics for biped walking robot. Robotics and Autonomous Systems 105, 1–10.

Johnson, A., Haynes, G., Koditschek, D., 2012. Standing self-manipulation for a legged robot, in: 2012 IEEE/RSJ International Conference on Intelligent Robots and Systems.

Johnson, A., Koditschek, D., 2013. Legged self-manipulation. IEEE Access 1, 310–334.

Johnson, M., Shrewsbury, B., Bertrand, S., Calvert, D., Wu, T., Duran, D., et al., 2017. Team ihmcs lessons learned from the darpa robotics challenge: finding data in the rubble. Journal of Field Robotics 34, 241–261.

Kajita, S., Espiau, B., 2008. Legged robots, in: Siciliano, B., Khatib, O. (Eds.), Springer Handbook of Robotics. first ed.. Springer, pp. 361–389.

Kamidi, V.R., Horn, J.C., Gregg, R.D., Hamed, K.A., 2021. Distributed controllers for human-robot locomotion: A scalable approach based on decomposition and hybrid zero dynamics. IEEE Control Systems Letters 5, 1976–1981.

Kant, N., Mukherjee, R., 2020. Orbital stabilization of underactuated systems using virtual holonomic constraints and impulse controlled poincar maps. Systems and Control Letters 164, 10481.

Kant, N., Mukherjee, R., 2022. Juggling a devil-stick: hybrid orbit stabilization using the impulse controlled poincar map. IEEE Control Systems Letters 6, 1304–1309.

Khadiv, M., Herzog, A., Moosavian, S.A.A., Righetti, L., 2020. Walking control based on step timing adaptation. IEEE Transactions on Robotics 36, 629–643.

Kim, D., Thomas, G., Sentis, L., 2014. Continuous cyclic stepping on 3d point-foot biped robots via constant time to velocity reversal. 13th International Conference on Control Automation Robotics and Vision, ICARCV 2014 .

Klavins, E., Koditschek, D., 2001. Stability of coupled hybrid oscillators, pp. 4200–4207.

Kvlcm, A., Karabacak, O., Wisniewski, R., 2021. Almost global stability of nonlinear switched systems with mode-dependent and edge-dependent average dwell time. Nonlinear Analysis: Hybrid Systems 41, 101052.

La Hera, P.X.M., Shiriaev, A.S., Freidovich, L.B., Mettin, U., Gusev, S.V., 2013. Stable walking gaits for a three-link planar biped robot with one actuator. IEEE Transactions on Robotics 29, 589–601.

Luck, J., Mehta, A., 1983. Bouncing ball with a finite restitution: chattering, locking, and chaos. Physical Review E 48.

Lynch, K.M., Northrop, M., Pan, P., 2001. Stable limit set behavior in a dynamic parts feeder. 2001 IEEE/RSJ International Conference on Intelligent Robots and Systems , 1129–1134.

Ma, W., Hamed, K.A., Ames, A.D., 2019. First steps towards full model based motion planning and control of quadrupeds: A hybrid zero dynamics approach, pp. 5498–5503.

Manchester, I.R., Mettin, U., Iida, F., Tedrake, R., 2011. Stable dynamic walking over uneven terrain. The International Journal of Robotics Research 30, 265–279.

Martin, A.E., Gregg, R.D., 2017. Stable, robust hybrid zero dynamics control of powered lower-limb prostheses. IEEE Transactions on Automatic Control 62, 3930–3942.

Mason, M., Salisbury, J., 1985. Robot hands and the mechanics of manipulation. Cambridge, MA, MIT Press.

Michel, A.N., 1999. Recent trends in the stability analysis of hybrid dynamical systems. IEEE Transactions on Circuits and Systems I: Fundamental Theory and Applications 46, 120–134.

Michel, A.N., Hu, B., 1999. Towards a stability theory of general hybrid dynamical systems. Automatica 35, 371–384.

Michel, A.N., Sun, Y., Molchanov, A.P., 2005. Stability analysis of discontinuous dynamical systems determined by semigroups. IEEE Transactions on Automatic Control 50, 1277–1290.

Moore, D., Shaw, S., 1990. The experimental response of an impacting pendulum system. International Journal of Non-Linear Mechanics 25, 1–16.

Moreau, J., 1988. Topics in nonsmooth mechanics. Birkhauser Verlag .

Morlando, V., Teimoorzadeh, A., Ruggiero, F., 2021. Whole-body control with disturbance rejection through a momentum-based observer for quadruped robots. Mechanism and Machine Theory 164, 104412.

Murray, R., Li, Z., Sastry, S., 1994. A Mathematical Introduction to Robotic Manipulation. CRC press.

Nguyen, H.N., Olaru, S., 2013. Hybrid modelling and constrained control of juggling systems. International Journal of Systems Science 44, 306–320.

Okamura, A., Smaby, N., Cutkosky, M., 2000. An overview of dexterous manipulation, in: 2000 IEEE International Conference on Robotics and Automation.

Ramezani, A., Hurst, J., Hamed, K., Grizzle, J., 2014. Performance analysis and feedback control of atrias, a three-dimensional bipedal robot. Journal of Dynamic Systems Measurement and Control-transactions of The ASME 136, 021012.

Ramirez-Alpizar, I.G., Higashimori, M., Kaneko, M., Tsai, C.D., Kao, I., 2012. Dynamic nonprehensile manipulation for rotating a thin deformable bbject: An analogy to bipedal gaits. IEEE Transactions on Robotics 28, 607–618.

Ruggiero, F., , Lippiello, V., , Siciliano, B., 2018a. Nonprehensile dynamic manipulation: A survey. IEEE Robotics and Automation Letters 3, 1711–1718.

Ruggiero, F., Petit, A., Serra, D., Satici, A., Cacace, J., Donaire, A., Ficuciello, F., Buonocore, L., Fontanelli, G.A., Lippiello, V., Villani, L., , Siciliano, B., 2018b. Nonprehensile manipulation of deformable objects: achievements

and perspectives from the robotic dynamic manipulation project. IEEE Robotics and Automation Magazine 25, 83–91.

Ryu, J., Lynch, K.M., 2018. Contact juggling of a disk with a disk-shaped manipulator. IEEE Access 6, 60286–60293.

Sanfelice, R., Teel, A., Sepulchre, R., 2007. A hybrid systems approach to trajectory tracking control for juggling systems. In Proceedings of 46th IEEE Conference on Decision and Control , 5282–5287.

Sardain, P., Bessonnet, G., 2004. Forces acting on a biped robot. center of pressurezero moment point. IEEE Trans. Syst. Man Cybernet. A 34, 630–637.

van der Schaft, A., Schumacher, J., 2000. An introduction to hybrid dynamical systems. Springer London 251.

Schill, M.M., Buss, M., 2018. Robust ballistic catching: a hybrid system stabilization problem. IEEE Transactions on Robotics 34, 1502–1517.

Serra, D., Ruggiero, F., Lippiello, V., Siciliano, B., 2017. A nonlinear least squares approach for nonprehensile dual-hand robotic ball juggling. IFAC PapersOnLine 50, 11485–11490.

Shiriaev, A.S., Freidovich, L.B., 2009. Transverse linearization for impulsive mechanical systems with one passive link. IEEE Transactions on Automatic Control 54, 2882–2888.

Spong, M., 2001. Impact controllability of an air hockey puck. Systems and Control Letters 42, 333345.

Spong, M.W., Holm, J.K., Lee, D., 2007. Passivity based control of bipedal locomotion. IEEE Robotics Automat. Mag. I 14, 30–40.

Su, H., Fang, Z., Xu, D., Tan, M., 2013. Trajectory prediction of spinning ball based on fuzzy filtering and local modeling for robotic pingpong player. IEEE Transactions on Instrumentation and Measurement 62, 2890–2900.

Surov, M., Shiriaev, A., Freidovich, L., Gusev, S., Paramonov, L., 2015. Case study in non-prehensile manipulation: planning and orbital stabilization of one-directional rollings for the butterfly robot, pp. 1484–1489.

Stre, C.F., Shiriaev, A.S., Freidovich, L.B., Gusev, S.V., Fridman, L.M., 2021. Robust orbital stabilization: A floquet theorybased approach. International Journal of Robust and Nonlinear Control 31, 8075–8108.

Tian, x., Koessler, J., Sanfelice, R., 2013. Juggling on a bouncing ball apparatus via hybrid control, pp. 1848–1853.

Turki, F., Gritli, H., Belghith, S., 2020. An LMI-based design of a robust state-feedback control for the master-slave tracking of an impact mechanical oscillator with double-side rigid constraints and subject to bounded-parametric uncertainty. Communications in Nonlinear Science and Numerical Simulation 82, 105020.

Vukobratovic, M., Borovac, B., Surla, D., Stokic, D., . Biped locomotion: Dynamics, stability, control, and application. New York: SpringerVerlag, 1990 .

Wendel, E.D., Ames, A.D., 2010. Rank properties of poincar maps for hybrid systems with applications to bipedal walking, pp. 151–160.

Westervelt, E.R., Grizzle, J.W., Chevallereau, C., Choi, J.H., Morris, B., 2007. Feedback Control of Dynamic Bipedal Robot Locomotion. CRC Press, Taylor and Francis Group, New York.

Wieber, P.B., Tedrake, R., Kuindersma, S., 2016. Modeling and control of legged systems, in: Siciliano, B., Khatib, O. (Eds.), Springer Handbook of Robotics. second ed.. Springer, pp. 1203–1234.

Woodruff, J.Z., Lynch, K.M., 2017. Planning and control for dynamic, nonprehensile, and hybrid manipulation tasks, in: 2017 International Conference on Robotics and Automation, pp. 4066–4073.

Xie, Z., Li, L., Luo, X., 2021. Three-dimensional aperiodic biped walking including the double support phase using lipm and lpm. Robotics and Autonomous Systems 143, 103831.

Yeganegi, M.H., Khadiv, M., Prete, A.D., Moosavian, S.A.A., Righetti, L., 2022. Robust walking based on mpc with viability guarantees. IEEE Transactions on Robotics doi:10.1109/TRO.2021.3127388.

Yi, Y., Lin, Z.Y., 2015. Stability and agility: biped running over varied and unknown terrain. Frontiers of Information Technology and Electronic Engineering 16, 283–292.

Zeng, D., Liu, Z., Chen, C.P., Zhang, Y., 2021. Event-triggered fuzzy adaptive control of nonlinear switched systems with predefined accuracy and mismatched switching. Fuzzy Sets and Systems .

Zhang, G., Ma, S., Shen, Y., Li, Y., 2020. A motion planning approach for nonprehensile manipulation and locomotion tasks of a legged robot. IEEE Transactions on Robotics 36, 855–847.

Zhang, H., Wang, H., Niu, B., Zhang, L., Ahmad, A.M., 2021. Sliding-mode surface-based adaptive actor-critic optimal control for switched nonlinear systems with average dwell time. Information Sciences 580, 756–774.

Zhang, K., Cao, Z., Liu, J., Fang, Z., Tan, M., 2018. Real-time visual measurement with opponent hitting behavior for table tennis robot. IEEE Transactions on Instrumentation and Measurement 67, 811–820.

Zhao, H., Horn, J., Reher, J., Paredes, V., Ames, A., 2017. First steps toward translating robotic walking to prostheses: a nonlinear optimization based control approach. Autonomous Robots 41, 725–742.

Zhu, H., Lu, J., Gu, S., Wei, S., Guan, Y., 2021. Planning three-dimensional collision-free optimized climbing path for biped wall-climbing robots. IEEE/ASME Transactions on Mechatronics 26, 2712–2723.